AIChE

A Particle-Scale Index in the Quantification of Mixing of Particles

G. R. Chandratilleke and A. B. Yu
Laboratory for Simulation and Modeling of Particulate Systems, School of Materials Science and Engineering, The University of New South Wales, Sydney, NSW 2052, Australia

J. Bridgwater
Dept. of Chemical Engineering and Biotechnology, University of Cambridge, Pembroke Street, Cambridge CB2 3RA, U.K

K. Shinohara
Particulate Chemical Engineering Laboratory, Chuo Ku, Sapporo, Hokkaido, 060-0051, Japan

DOI 10.1002/aic.12654
Published online May 25, 2011 in Wiley Online Library (wileyonlinelibrary.com).

Discrete element method (DEM) is a useful tool for obtaining details of mixing processes at a particle scale. It has been shown to satisfactorily describe the flow structure developed in bladed mixers. Here, the advantage is taken of the microstructure gained from DEM to evaluate how best to quantify the microstructure created by mixing. A particle-scale mixing index (PSMI) is defined based on coordination numbers to represent the structure of a particle mixture. The mixture quality is then analyzed qualitatively and quantitatively in three different ways: a macroscopic mixing index based on the conventional approach, coordination number, and PSMI. Their effectiveness is examined based on DEM data generated for different particle loading arrangements and binary mixtures of particles with various volume fractions, size ratios, and density ratios. Unlike the two other methods, PSMI reveals in a straightforward manner whether a binary mixture of different particles is mixing or segregating over time, while being able to detect particle-scale structural changes accompanying the mixing or segregation processes in all the mixtures investigated. Moreover, PSMI is promising in that it is not influenced by the size and number of samples, which afflict conventional mixing indexes. © 2011 American Institute of Chemical Engineers *AIChE J,* 58: 1099–1118, 2012
Keywords: powder mixing, coordination number, mixing index, discrete element method, granular dynamics

Introduction

Particle mixing is an important operation used in many industries to obtain products with controlled properties. Some such examples are pharmaceuticals, such as tablets and capsules,[1] high-hardness composite materials for cutting tools,[2] and masses of polymers, known as resins in the manufacture of plastics,[3,4] and functional cosmetic materials made by coating particles with powders.[5] In all these products, uniformity of particle mixtures is crucial. For example, in the pharmaceutical industry, quality control of the mixed material is very important. If the product variation is beyond specified limits, a batch of products will be discarded, to comply with regulations.[1] Such procedures are needed to

Correspondence concerning this article should be addressed to A. B. Yu at a.yu@unsw.edu.au.

protect consumers from possible health risks because poor quality can cause different drug-release rates with possible side-effects on consumers. In addition, production costs may rise if tablets are prone to crumbling in the manufacturing process because of nonuniformity in the structure. Therefore, the overall quality of a mixture is understood to be crucial for all the parties concerned. Similar consideration is applicable to many other applications. For example microscale mixing is shown to improve the strength of a tool-making compound, which consists of alloyed WC–Co particles and a mixture of TiC and Al_2O_3 coating particles. Similarly, particle-scale mixing has been shown to be important in the cosmetic industry for improving the efficiency of sunscreen lotions, while avoiding skin irritation.[5]

Thus, it is important to consider the appropriate scale of scrutiny in accordance with the process. Although this importance has also been stressed previously,[6,7] only a limited number of studies can be found in relation to mixing at a particle scale. Akao et al.[8] pointed out the need to define a mixing index that reflects the structural effects of a particle bed. They observed that (i) macroscopic indexes do not provide significant insight into the microscopic and geometric nature of the mixture and (ii) there are difficulties in applying such definitions to a regular (or an ordered) packing arrangement, which will result in an inaccurate sample variance. To overcome these drawbacks, they defined a degree of mixing M based on coordination numbers as follows.[8]

$$M = \frac{\hat{C} - E[C_{A(B)}]_{seg}}{E[C_{A(B)}]_{rand} - E[C_{A(B)}]_{seg}} \quad (1)$$

where $C_{A(B)}$ is the coordination number, namely the number of contacts of a key particle of B-type with A-type particles; $\hat{C}$ is an estimate of the average value of $C_{A(B)}$ for the mixture based on samples drawn from the mixture. $E[C_{A(B)}]_{\mathrm{seg}}$ is the expected value or the mean of the distribution of the variable $C_{A(B)}$ in the segregated state of the mixture. $E[C_{A(B)}]_{\mathrm{rand}}$ is the expected value of the variable $C_{A(B)}$ in the random state of the mixture. M varies from 0 to 1, when the mixture changes from a segregated state to random or well-mixed state. They conducted numerical experiments at the fully random state of binary mixtures of monosized particles for several mixing fractions. They also calculated M for the cases in which the particles are randomly distributed in cubic and hexagonal structures. Their results show that M depends on the mixture structure, with the hexagonal structure showing a better mixed state than the cubic structure at a given mixing fraction. Therefore, their work demonstrates that the mixing index based on contact number is indeed structure-dependent. Contrarily, a macroscopic index would have produced mostly identical results for the two structures.

Akao et al.[9] also demonstrated by numerical experiments that an estimator of a mean value such as $\hat{C}$ in Eq. 1 produces a smaller relative standard error (RSE) than an estimator of a variance when using the sampling approach, where RSE is defined as the ratio of the standard deviation to the mean value of the estimator. Therefore, they concluded that the mixing index of Eq. 1 based on mean values is superior to the commonly used mixing indexes such as Lacey index based on variances.[10] They also showed that RSE decreases with the increase of the number of samples in both methods, but the variance method requires a larger number of samples to reduce RSE.

Recently, a new mathematical method has also been developed to evaluate the degree of mixing of particle systems by Siiriä et al.[11] According to them, the method requires the knowledge of the locations of some or all of the particles in a mixture both before and after mixing. The degree of mixing is calculated using the changes in the distances of the particles with respect to the original positions. Although it is a particle-scale index, it is more related to particle-scale dispersion than that to the structure of the mixture. Further, its applicability has been demonstrated only for monosized particles.

It has not been feasible to pursue particle-scale investigations with practical systems because there is no way of gaining the information required experimentally, at least at this stage of development. However, it is now possible to gain such information from modeling of particle mixers by means of the discrete element method (DEM), which is well supported by the positron emission particle tracking (PEPT) method,[12,13] in which detailed measurements on particle position and velocity are made. Indeed, DEM has been used increasingly in the study of powder mixing in recent years as reviewed by Zhu et al.[14] In particular, Zhou et al.[15] used DEM to investigate the flow and mixing of monosized particles in a two-bladed vertical cylindrical mixer. These authors also examined the mixing or segregation mechanisms of binary mixtures of particles with either a size or density difference.[16] For a similar mixer, Chandratilleke et al.[17,18] investigated the effects of variables such as blade speed, blade rake angle, and clearance. On the other hand, Remy et al.[19,20] investigated the flow and mixing of monosized particles in a four-bladed vertical cylindrical mixer by DEM, focusing on the effects of wall roughness, blade speed, blade orientations, and fill level. The role of convective and diffusive mixing was also examined.[19] Recently, Radeke et al.[21] showed that DEM can be used in combination with graphics processing unit technology to investigate mixing of several millions of particles in a similar mixer, thus taking DEM further closer to solving practical mixing problems. However, in the studies thus far reported, the quantification of mixing behavior has been based on the conventional mixing indexes such as Lacey index or RSE, which may be problematic as discussed above. How to devise a mixing index to make a full use of the particle scale information generated by DEM simulations is still a challenging problem.

The aim of this article is to present our approach to this problem. In particular, use is made of data on the structural evolution of particles as a function of mixing time obtained from DEM simulations to gain the contact information. Thus, the evaluation of the mixture quality can be obtained by using many samples that contain a large number of particles. Similarly, the coordination number for each particle can also be used as found or used in new relationships in the assessment of the mixture quality. The effectiveness of such methods of assessing mixture quality is thus provided for the mixing of like particles and binary particles with difference in relative amount, size, and density.

Methods to be Evaluated

Many mixing indexes have been developed to quantify granular mixing and segregation.[22] Here, we consider an

index defined in terms of segregation index (also known as intensity of segregation), which is suitable for the macroscopic scale. To investigate mixture quality at a particle scale, two approaches are used, one involving coordination number and the other involving a particle-scale index derived from coordination numbers.

Macroscopic mixing index

A macroscopic mixing index M can be defined as,[23]

$$M = 1 - I \tag{2}$$

where I is the segregation index for a binary mixture, defined by the following equation[6,24,25]:

$$I = \frac{\sigma_t^2}{\sigma_0^2} \tag{3}$$

Here, σ_t is the standard deviation of particle fraction of one type of particles in samples at time t; σ_0 is the value of σ_t, when the particles are in the fully segregated state at some time $t = t_0$, and σ_t and σ_0 are defined according to the following equations:

$$\sigma_t^2 = \frac{\sum_{i=1}^{i=N_0} w_i (x_i - \bar{x}_t)^2}{\sum_{i=1}^{i=N_0} w_i} \tag{4}$$

$$\bar{x}_t = \frac{\sum_{i=1}^{i=N_0} w_i \, x_i}{\sum_{i=1}^{i=N_0} w_i} \tag{5}$$

and

$$\sigma_0^2 = p(1-p) \tag{6}$$

where x_i is the number fraction of particles of a target type in sample i, $\bar{x}_t$ is the instantaneous value of the particle fraction x_i averaged over all the samples N_0 based on Eq. 5 at time t, $w_i = V_i/V_T$ is the weighting used in the above averaging operations[18] and is defined as the fraction of the particle volume of sample i to the total volume V_T of the particles in the mixture (with $\sum_{i=1}^{N_0} w_i = 1$), and p is the overall particle number fraction of the target type particles considered. Note that Eq. 6 is applicable to binary sized particles at the segregated state.[10,25]

As particles are laid initially in a segregated arrangement, the calculated value of σ_t at $t = t_0$ is very close to σ_0 in the simulations to follow. However, it is also possible that σ_t at $t = t_0$ be slightly smaller than σ_0 because of the apparent mixed state that results if one type of particles are either few in number or smaller in the size than the other type. Therefore, it is reasonable to say that I is close to 1 or M is close to zero for the fully segregated state at $t = t_0$ as seen from Eqs. 2 and 3, respectively. When mixing takes place, σ_t is ideally expected to reduce and reach a small value. In other words, I should decrease or M increases when mixing proceeds. In the case of an ideally mixing mixture such as a binary mixture of uniform particles in terms of either density or size, σ approaches σ_r corresponding to the fully mixed state given by the equation:

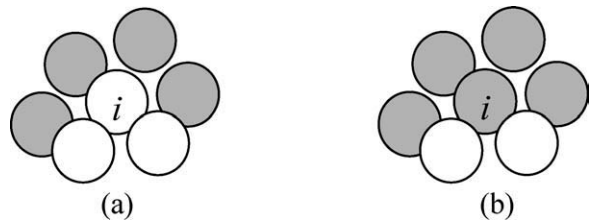

Figure 1. A group of particles in contact with particle *i*: (a) core particle *i* is *W*-type, (b) core particle *i* is *B*-type.

$$\sigma_r^2 = \frac{p(1-p)}{n} \tag{7}$$

where n is the sample size or number of particles in each sample and p is the overall particle number fraction of the target type particles based on particle numbers.[10,22] Therefore, based on Eqs. 2, 6, and 7, for the ideal mixture M approaches $(1 - 1/n)$, which is close to 1, if the sample size n is large enough. Hence, M as defined in Eq. 2 varies between roughly 0 and 1 when the mixture changes from the fully segregated state to the fully mixed state.

Coordination number

The coordination number of a particle is defined as the total number of particles that are in contact with the particle. A particle is considered to be in contact with another if the gap between their surfaces is less than a certain value. Here, unless otherwise specified, this critical value is set to 5% d, where d is particle diameter of the smaller particle if a binary mixture is considered. If a mixture is multicomponent, the coordination number can be broken down into partial coordination numbers to represent different types of contacts.[26,27] Therefore, the coordination or contact numbers provide a second method of investigating mixing at a particle level.

Particle-scale index

Here a new method of quantitatively analyzing the microscopic structure of a mixture is proposed. It relies on the use of the coordination number gained at the particle level. Figure 1 shows schematically the particles in contact with particle i in a binary mixture. Particle i can either be of W-type (white) or B-type (black), respectively, as shown in Figures 1a, b. If core particle i is a W-type particle, the particle number fraction p_i of the target type particle B in contact with particle i can be obtained as follows:

$$p_i = \frac{Cn_{B(W)}}{Cn_i + 1} \tag{8}$$

where $Cn_{B(W)}$ is the number of B-type contacts (or contact number) for the core particle i of W-type, and Cn_i is the total

coordination number of particle i. In this work, a particle is assumed to be in contact with particle i if it forms a gap of 5% d or less with particle i, where d is the diameter of the smaller of the two types of particles.

On the other hand, if the core particle i is of B-type, the particle fraction p_i of the B-type particles in contact with particle i can be obtained as follows:

$$p_i = \frac{Cn_{B(B)} + 1}{Cn_i + 1} \tag{9}$$

where $Cn_{B(B)}$ is the number of B-type contacts for the B-type particle i, and Cn_i is the total coordination number of particle i. To find local particle fraction using Eq. 8 or 9, one has to select the type of core particle i first.

To define a particle-scale degree of mixing, consider the definition of Lacey's mixing index, which is valid literally for a uniform particles[10]:

$$M = \frac{\sigma_0^2 - \sigma_t^2}{\sigma_0^2 - \sigma_r^2} \tag{10}$$

Here, ${\sigma_t}^2$, ${\sigma_0}^2$, and ${\sigma_r}^2$ are the variance terms defined in Eqs. 4, 6, and 7, respectively. These are dependent on macroscopic quantities. For example, ${\sigma_t}^2$ depends on the average particle fraction $\bar{x}_t$ of the mixture, ${\sigma_0}^2$ on p, and ${\sigma_r}^2$ on both p and the sample size n.

Now, let the particle-scale mixing index (PSMI) or degree of mixing M be defined by analogy to Lacey's mixing index of Eq. 10 as follows:

$$M = \frac{S_0^2 - S_t^2}{S_0^2 - S_R^2} \tag{11}$$

The equation uses the particle-scale variance ${S_t}^2$ of particle fraction p_i with the particle-scale variances ${S_\mathrm{R}}^2$ and ${S_0}^2$ of the two reference states, fully mixed and fully segregated, respectively. ${S_t}^2$ can be found using Eqs. 12 and 13 together with the definitions for p_i in Eqs. 8 and 9.

$$\bar{p}_\mathrm{t} = \frac{1}{N}\sum_{i=1}^{i=N} p_i \tag{12}$$

$$S_\mathrm{t}^2 = \frac{1}{N}\sum_{i=1}^{i=N} (p_i - \bar{p}_\mathrm{t})^2 \tag{13}$$

Here, N is the total number of particles in the mixture. The average particle fraction $\bar{p}_\mathrm{t}$ in Eq. 12 is the average value of p_i, and S_t in Eq. 13 is the standard deviation of the instantaneous frequency distribution of p_i for the mixture.

It remains to obtain the particle-scale values ${S_0}^2$ and ${S_\mathrm{R}}^2$. The macroscopic quantity ${\sigma_0}^2$ of Eq. 6 is independent of the sample size n, and, therefore, ${S_0}^2$ can be made equal to ${\sigma_0}^2$.

$$S_0^2 = \sigma_0^2 \tag{14}$$

On the other hand, the variance for the fully mixed state ${S_\mathrm{R}}^2$ is not known for a binary mixture of different sized particles. Therefore, we take here the reference well-mixed state as the well-mixed state of monosized particles with the same particle number ratio p as that of the binary mixture. This definition will provide consistency with the case of monosized particles. Therefore, ${S_\mathrm{R}}^2$ is defined by the following equation:

$$S_R^2 = \frac{p(1-p)}{n} \tag{15}$$

Here, n is a particle-scale sample size and is chosen as 7, which is equivalent to: 1 + the average coordination number of monosized particles (Figure 3). Note that, the value chosen for n in the above equation has an effect on the final value of M. As stated before, the particle fraction p at the particle scale under the well-mixed reference state is chosen as the number ratio of the target type particles in the binary mixture.

It should be noted that the particle-scale mixing index according to Eq. 11 is associated with the structure of the mixture because of the coordination numbers used in Eqs. 8 and 9. If the structure is such that the particles are segregated, then Eq. 11 shows that M should be close to zero as a result of S_t being close to S_0. When the structure of the mixture changes, the coordination numbers in Eqs. 8 and 9 change, reflecting those changes in S_t, and, therefore, in M of Eq. 11 as well. If the mixture reaches a structure similar to that at the fully mixed state of a monosized particle mixture, S_t becomes roughly equal to S_R, making M nearly 1.

In the definition of mixing index, we have used the variance despite the statement of Akao et al.[9] that a variance-based approach produces larger errors. Such errors would indeed occur when spot-sampled information is used for predictions.[9,28] However, the present definition of Eq. 11 does not use the population values predicted by a spot sampling method. Rather, it uses the directly evaluated population mean values. Therefore, the variance based method used here will not introduce prediction errors.

Simulation Model

DEM is used to simulate mixing in a vertical-axis cylindrical mixer with a two-bladed impeller. The blades have their broader surfaces vertical. The DEM model was verified in a previous work[15] by comparison with the results generated by PEPT, which is also a particle-scale approach. The model is formulated by considering the conservation of momentum in both the translational and rotational motion of all the particles in the system. When a particle makes a contact with another or a wall, it experiences both elastic and damping forces at the contact point in both normal and tangential directions to the contact surface. The particle also experiences torque because of the tangential forces and rolling friction, which is linked to energy dissipation within the material caused by the deformation of the particle on rolling. These forces and torques determine the particle motion under the governing principle of conservation of momentum. Zhu et al.[29] recently reviewed the DEM approach in detail. The present DEM work follows the approach we reported recently,[18] and it is not repeated here for brevity.

Simulation Conditions

The mixer construction used for this study is similar to that of Stewart et al.[12] The mixer consists of a vertical cylindrical vessel and a pair of flat blades, which are attached to

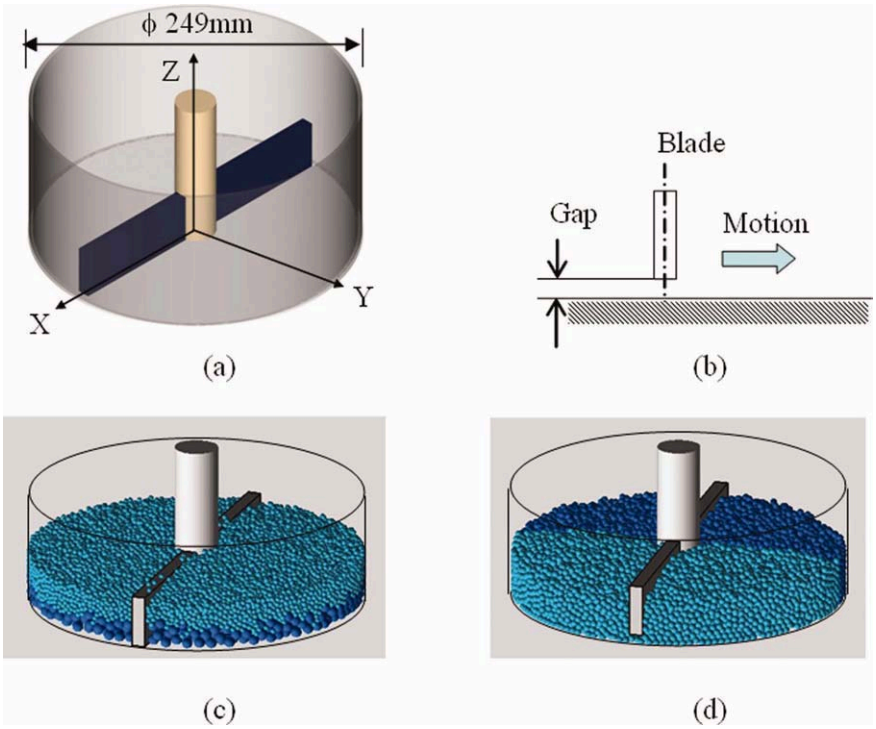

Figure 2. (a) Geometry of the mixer used in the simulation, (b) definition of gap at vessel bottom for a single blade, (c) initial particle arrangement for top-bottom (T–B) loading, and (d) initial particle arrangement for side-by-side (S–S) loading.

[Color figure can be viewed in the online issue, which is available at wileyonlinelibrary.com.]

an axial shaft at diametrically opposite positions so that the wide sides of the blades are vertical as shown in Figure 2. The vessel has an inner diameter of 249 mm and the axial shaft of the mixer has a 32-mm diameter. The blades are each 40 mm in width, 10 mm in thickness, and 106 mm in length. The clearance of the blades at the vessel wall is 2.5 mm and that at the bottom is listed for each case study, in Table 1. Two initial particle arrangements used in this study are shown in Figures 2c, d, and that used in each case study is listed in Table 1.

The particles are spherical with properties close to those of glass beads.[15] In addition, the properties of the mixer walls and blades are assumed to be identical to those of the particles. The physical properties used in the simulation are as follows: rolling friction coefficient, $\mu_r = 5 \times 10^{-5}$ m; sliding friction coefficient, $\mu_s = 0.3$; particle density, $\rho = 2500$ kg/m^3; Poisson ratio, $v = 0.3$, and damping coefficient, $c = 0.3$. However, Young's modulus has been reduced from 10^9 N/m^2 of real glass beads to 2.16×10^6 N/m^2 to reduce the time step in the computations, and results of this approach have been found to compare well with experimental results.[12,17] The time step used is between 2 and 5×10^{-6} s, and computation time on a server (8 CPU, Intel Xeon, 2.5 GHz, 8 GB RAM) is about 10 min for 0.01 s on the time axis of simulation. The possible effect of air on mixing is neglected because the blade and particles are moving at low speeds and particles are large.

A simulation is started by random generation of spheres of a specific diameter in a layer without any overlaps and then dropping that layer of particles. When the falling layer clears off its original position, another layer is generated in the same position and dropped. This process is continued

Table 1. Details of simulation cases*

Case	d_1 (mm)	d_2/d_1	N_1	N_2	N_1:N_2	Blade Gap, G (mm)	$\alpha = V_1/(V_1+V_2)$	Loading Pattern
1	5.0	1	8750	8750	1:1	7.5	0.5	T–B
2	5.0	1	8747	8753	1:1	7.5	0.5	S–S
3	8.0	0.5	395	28,462	1:72	0	0.1	T–B
4	8.0	0.5	2000	15,625	1:7.81	0	0.5	T–B
5	8.0	0.5	3558	3163	1:0.89	0	0.9	T–B
6	4.98	0.95	8194	9443	1:1.15	0	0.5	T–B
7	4.98	0.90	8194	11,240	1:1.37	0	0.5	T–B
8	4.98	0.8	8190	16,000	1:1.95	0	0.5	T–B
9	5.0	1	8000	8000	1:1	0	0.5	T–B

*Subscripts 1 and 2 represent the types of particles; d, N, V, and α represent diameter, particle number, total volume of one type of particles, and volume fraction, respectively; S–S indicates side-by-side loading; T–B indicates top–bottom loading; and particle properties are stated in Simulation Conditions section.

until the total number of particles dropped reaches the required total particle number. Then, particles are allowed to settle down under the gravity for approximately 0.8–0.95 s. Immediately after the settling, the shaft-blade unit is rotated at 20 rpm. The mixtures and their loading arrangements are listed in Table 1. The loading arrangements T–B and S–S are shown in Figure 2. Another arrangement used is the "S–S rotated" arrangement, which is produced by rotating the particle-group interface in the S–S arrangement by 90° and making it parallel to the blades.

To evaluate σ_t^2 in Eq. 4, one needs to extract samples from the mixture. To do so, the mixing space of the vessel is divided into several axis-symmetric cells. The division of the mixing space into cells is done as follows. In the radial direction, four concentric cylinders divide the space between the shaft and vessel wall into five annular cylindrical spaces, each space having a width of 21.7 mm. In the circumferential direction, several radial planes divide each annular cylinder equally, the number of segments for each annular cylinder being 6, 11, 16, 21, and 26 from the innermost (near the shaft) to outermost annular cylinder, respectively. In the axial direction, horizontal planes spaced at 20 mm divide the already divided segments to form cells of equal height. The sample size, that is, the number of particles in a sample, varies, which will give different weights in the calculation of σ_t^2.

Results and Discussion

Mixing of uniform particles

A study of the mixing of uniform particles provides us an opportunity to investigate mixing mechanisms peculiar to a mixer because of the absence of the effects due to the differences in particle properties. This section presents the results for the mixing of such particles under the conditions corresponding to Cases 1 and 2 in Table 1. The three methods of analysis are considered in turn.

Macroscopic Index There are two major mixing mechanisms in a bladed mixer: convective mixing (bulk motion of particles) and diffusive mixing (random motion of particles).[19,30–32] The convective mixing is the dominant mechanism in the present mixer, as it has been confirmed previously for a similar type of mixer.[20] Figure 3 shows the variation of the macroscopic mixing index as a function of mixing time for the two loading conditions: top–bottom (curve 1) and side-by-side (curve 2). The mixing index shows some fluctuations at the start of mixing; in this period, the moving blades gradually set particles in a convective motion. The mixing index gradually increases with mixing time. Initially separated, corresponding to the initial layouts of particles, the two values become similar for a period of time before separation. The S–S arrangement results in a slightly larger mixing index after 20 s than the top–bottom arrangement. This difference gradually narrows in the approach to the steady state. It is also observed from the animations that movement of a particle is slightly hampered if a particle gets into the gap between the blade tip and vessel walls, where there is a clearance of 2.5 mm; however, particles flow under the blades without any difficulty, having a gap of 7.5 mm at the vessel bottom. Therefore, some occasional particle jamming effect can be observed near the blade tip.

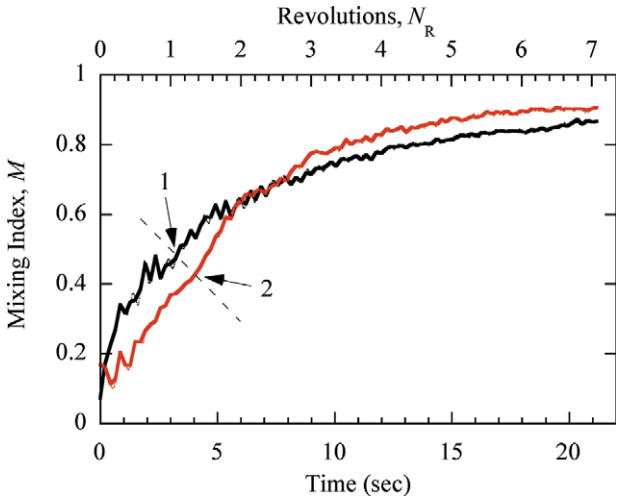

Figure 3. Macroscopic mixing index as a function of mixing time: curve 1 is Case 1 and curve 2 is Case 2.

[Color figure can be viewed in the online issue, which is available at wileyonlinelibrary.com.]

Coordination Number In the two loading arrangements, consider one group of particles being colored black (B) and the other white (W), with B-particles being at the mixer bottom in the top–bottom (T–B) arrangement for the purpose of discussion below. Mixing is started after a settling time of 0.95 s. When mixing progresses, four types of particle contact appear, namely, B–B, W–W, W–B, and B–W contacts, where the first letter represents the color of the core particle and the second represents that of a particle in contact with the core particle. For each core particle of B type in the mixture, we can break down its total number of contacts into B–W and B–B type contact numbers; similarly, for each core particle of W type, its total number of contacts can be broken down into W–W and W–B type contact numbers. Thus, these yield frequency distributions of the each contact type at any instant of the mixing process. In obtaining such distributions, one must consider only the core particles with one or more contacts in each type of contact. To find the average number of B–W contacts per B core particle, the B-particles that have B–W contacts are used. This procedure excludes the B-particles that have only B–B contacts.

Figure 4 shows the average of each frequency distribution as a function of time. Figures 4a, b correspond to the side-by-side and top–bottom initial arrangements, respectively. Both figures show that the total average coordination number initially reduces but remains unchanged thereafter with almost identical values. Thus, bed dilation occurs as soon as the blades start moving but remains unchanged with time because of the repetitive nature of the bed dilation process as the blades move. The bed dilation should thus be independent of the initial particle arrangement as the figures confirm.

On the other hand, both W–W and B–B coordination numbers reduce in an identical manner when mixing progresses, and become steady when the mixture reaches fully mixed or randomized state in each case. For the side-by-side arrangement (Figure 4a), both B–W and W–B coordination numbers increase as mixing progresses and reach a steady value that is almost the same as for the W–W or B–B

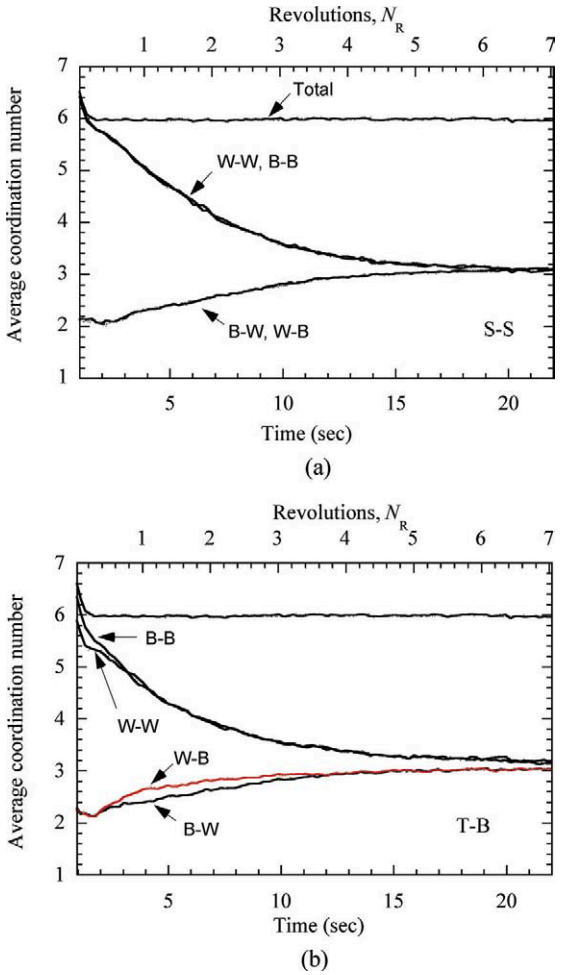

Figure 4. Average coordination number as a function of time, at $G = 1.5\,d$, where d is particle diameter: (a) side-by-side loading of particles and (b) top–bottom loading of particles.

[Color figure can be viewed in the online issue, which is available at wileyonlinelibrary.com.]

coordination numbers; this behavior arises because the mixing fraction is roughly 0.5. However, for top–bottom arrangement, as shown in Figure 4b, the traces of W–B and B–W contacts show slight differences. This can be explained as follows. B-particles at the bottom of vessel are being pressed by the moving blade, and as a result, the average porosity among B-particles is less than that among the W-particles, which are laid on top of the W-particles. Therefore, W-particles penetrate with difficulties into B-particle region at the bottom, whereas B-particles penetrate more readily into the W-particle region at the top. As a result, there will be less W-particles in the B-particle region than B-particles in the W-particle region. Thus, the total B–W and W–B contacts in the mixture being identical, the average W–B contacts per W-particle should be greater than the average B–W contacts per B-particle.

Taking the argument further, consider the probability distributions of B–W and W–B contact numbers at $t = 4$ s in Figure 5, when the difference between B–W and W–B

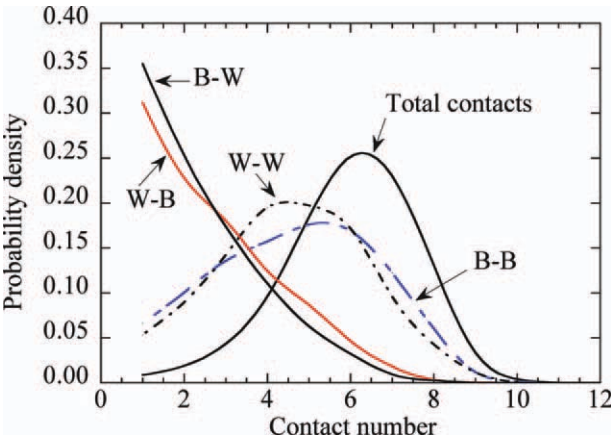

Figure 5. Probability density distributions of contact numbers at $t = 4$ s for top–bottom initial arrangement in which W-particles are on top of B-particles.

[Color figure can be viewed in the online issue, which is available at wileyonlinelibrary.com.]

contacts as seen from Figure 4b is larger. The average value of W–B contacts is larger than that of B–W contacts, because the area under the W–B curve is larger than that under B–W curve. More specifically, the B–W and W–B contacts are each equal to 12,920, but the total of W core particles having B contacts is 4823, whereas the total of B core particles having W contacts is 5335. Therefore, a W core particle has B contacts equal to 12,920/4823 on average, while a B core particle has W contacts equal to 12,920/5335 on average. Thus the W–B contact numbers are larger than B–W contact numbers although the total numbers of B–W and W–B contacts are identical. The figure also shows that B–B contacts have a large average value than W–W contacts, which indicates that B-particles at the bottom are in a more compact state than W-particles at the top due to the action of the blade and gravity.

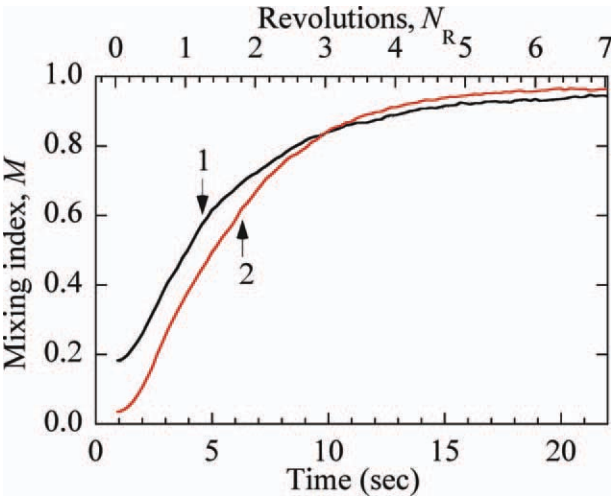

Figure 6. Particle-scale index as a function of time: curve 1 is Case 1 and curve 2 is Case 2.

[Color figure can be viewed in the online issue, which is available at wileyonlinelibrary.com.]

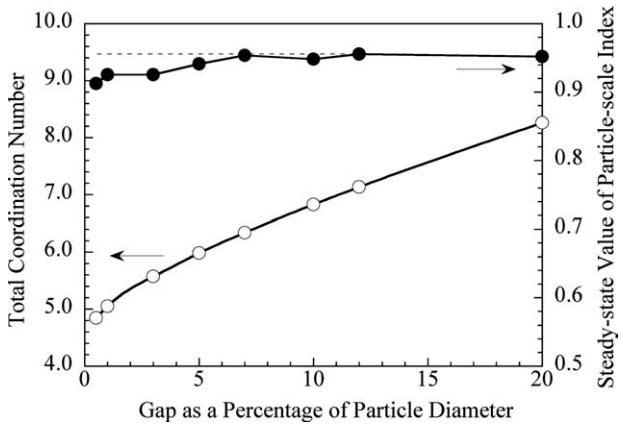

Figure 7. Steady-state values of total coordination number and particle-scale index for Case 1 as functions of inter-particle gap size.

Because of this contact difference occurring at initial stages of mixing, the top–bottom arrangement will take a longer time to converge to the steady state level than the side-by-side arrangement. Figure 4a shows that the steady-state is reached in about 20 s in the side-by-side arrangement, whereas Figure 4b shows that it takes longer than 22 s for the top–bottom arrangement. This result is in agreement with the discussion of macroscale mixing shown in Figure 3.

Particle-Scale Index To analyze the mixing behavior using this index, an instantaneous distribution of particle-scale particle fraction is first established by arranging the particles fractions found from Eqs. 8 and 9 in a distribution. Then, the dispersion of the distribution as defined by Eq. 13 is determined in combination with Eq. 12. Figure 6 shows the particle-scale index M (Eq. 11) for the top–bottom and side-by-side arrangements, respectively, corresponding to Cases 1 and 2 in Table 1. The top–bottom arrangement (curve 1) shows initially a higher M than Case 2 but indicates a less complete mixing after 20 s. Similar effects were observed in Figure 3. In Case 1, there is a larger initial interfacial area as seen from a comparison of Figures 2c, d. The larger contact area causes the initial value of M to be larger. However, the poor particle mixing at the bottom delays mixing at a later time. Some differences can be observed in M at the macro and particle scales as seen from a comparison of Figures 3 and 6. The PSMI M fluctuates only very slightly, the cross-over point of the curves is sharply defined and occurs later at about 10.5 s.

Consider the RSE, $S_t/\bar{p}_t$. At steady-state, the results show that S_t^2 for the side-by-side case is 0.0434, and a rough value for $\bar{p}_t$ can be found as 4/7 using the average B–B and the total coordination numbers of Figure 4a in Eq. 9. Conversely, S_R^2 of Eq. 15 at the particle-scale is found to be 0.0354 considering a sample size of seven particles with the mixing ratio p of 0.546 (for Case 2). Thus, RSE in terms of $S_t/\bar{p}_t$ is 0.364, whereas it is 0.344 in terms of S_R/p. The smaller the RSE, the greater the order in the particle arrangement of the mixture at the particle-scale. Therefore, one can conclude that although the vertical blade-mixer can mix particles well, the resulting mixture is not greatly ordered at the particle-scale.

At large mixing times, the differences between Cases 1 and 2 diminish. The attainment of nearly 1 for M suggests that the vertical bladed mixer has performed its function of randomizing the particles well for uniform particles. Therefore, we can expect that no significant improvement to the quality of the mixture will happen even if we use more blades in the mixer. However, the use of several blades can reduce the mixing time,[33] which is important when mixing a large number of particles.

At this point, it should be pointed out that the particle-scale index may be affected by the value of the gap used to define the contact between particles. To investigate this effect, the gap size is varied from 0.5 to 20% for Case 1. As shown in Figure 7, the overall coordination number monotonically increases with the increase of the gap size; this result is consistent with those reported in the literature. The particle-scale index gives a similar trend, but not so sensitive. Nonetheless, the results suggest that to be comparable, it is important to use a consistent gap size in determining the coordination number and hence the particle-scale index. This explains why a fixed gap size, that is, 5% d, is used in this work.

Effect of Loading Pattern and Blade Clearance Here monosized uniform particles are used to investigate the combined effect of loading and blade clearance on mixing. As demonstrated in Figures 3 and 6, mixing indexes at different scales produce comparable behavior for such particles. Therefore, for convenience, we just use the particle-scale index in the present analysis. Case 2 is used to produce the results for $G = 1.5\ d$ with particles loaded in the side-by-side (S–S) pattern; here G is the blade clearance at the vessel base. Case 9 is used to produce the results for $G = 0$ with particles loaded in the T–B, S–S, and S–S rotated arrangements.

The particle-scale index is shown in Figure 8 as a function of time for each of the above combination of the loading pattern and blade clearance. The initial states of mixing are

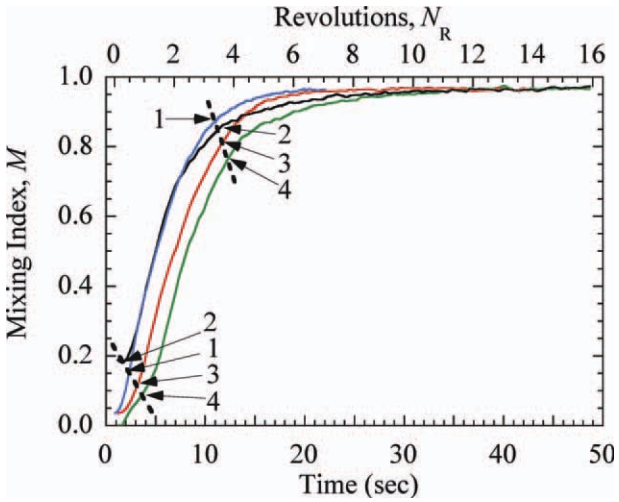

Figure 8. Effects of loading pattern and blade clearance on mixing of uniform particles at 20 rpm.

Curve 1, S–S arrangement with $G = 1.5\ d$ (Case 2); curve 2, T–B arrangement with $G = 0$; curve 3, S–S arrangement with $G = 0$; and curve 4, S–S rotated arrangement with $G = 0$. [Color figure can be viewed in the online issue, which is available at wileyonlinelibrary.com.]

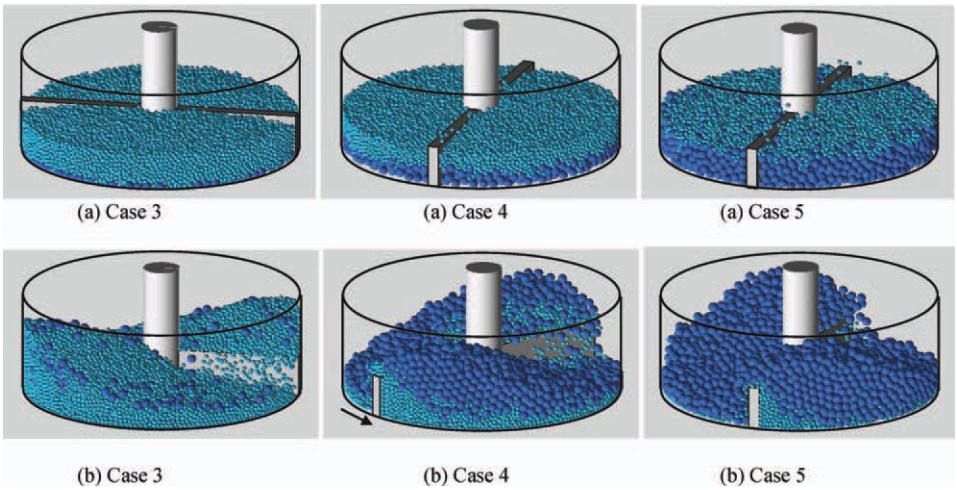

Figure 9. Initial and final states of the binary mixtures of Cases 3–5.

Top row (a) represents the initial top–bottom particle arrangements at 0.8 s just close to the start of mixing and bottom row (b) represents the states at the end of mixing at 9.6, 14.6, and 17.3 s for Cases 3–5, respectively. The arrow shows the common direction of motion of blade. [Color figure can be viewed in the online issue, which is available at wileyonlinelibrary.com.]

different depending on the initial particle arrangement and G because of the differences in the area of the interface between the two types of particles. The figure shows that curve 2 (T–B) has the largest initial M value, the particles being loaded in T–B arrangement, in which the two types of particle have the largest interfacial area. On the other hand, curve 4 (S–S rotated) has the lowest initial M value, the particles being completely separated by the blades. The initial rate of mixing is similar for each condition, but the rate becomes different from each other after about 10 s.

Considering the time to reach the steady-state M value, curve 4 (S–S rotated, $G = 0$) takes the longest time of all the conditions as seen from Figure 8. Therefore, it has the slowest mixing rate of all the conditions. Such a slow rate can be inferred from the flow patterns that have been reported previously.[15] These flow patterns are such that when viewed relative to the blades, the particles that recirculate in front of the blade are large in number in comparison with those that flow over the blade at the blade speed considered. Therefore, the particle recirculation in front of the blade does not promote the mixing in the S–S rotated arrangement. A comparison of curve 3 (S–S, $G = 0$) with curve 4 (S–S rotated, $G = 0$) shows that S–S arrangement is much faster in reaching the steady-state that S–S rotated arrangement. The reason for this improvement is followed from the above argument of recirculating flow pattern. On the other hand, curve 2 (T–B, $G = 0$) shows larger M values than curve 3 (S–S, $G = 0$) before about 12 s due to the similar argument, but it delays in reaching the steady-state. This delay is caused due to the reason used to explain the results in Figure 6. As seen from the results for $G = 0$, the loading arrangement has an effect on the overall mixing rate, with S–S arrangement showing the fastest rate. Such trends in the mixing curves have also been observed previously, where the Lacey index is used.[10] Therefore, the above results show that the particle-scale index can produce results consistent with the macroscopic mixing index for mixing of uniform particles.

Now, a comparison of curve 1 (S–S, $G = 1.5d$) with curve 3 (S–S, $G = 0$) in Figure 8 shows that curve 1 has the fastest overall mixing rate of all the conditions, despite the fact that it corresponds to a larger number of particles. Therefore, value of G has a significant effect on the overall mixing rate. The blade clearance will allow some particles to pass under the blades improving mixing, although the dominant flow pattern at this blade speed is the recirculation flow. However, we have also shown previously that use of excessively larger blade clearances can reduce the mixing rate under T–B loading condition.[17] Finally, the figure also shows that neither the particle loading arrangement nor the blade clearance has an effect on the final (steady) state of mixing.

Mixing of binary particles: effect of volume fraction

Mixtures of particles of different sizes are prone to segregate. The mixing behavior of binary mixtures depends on the flow field, volume fraction, and sizes of particles under given conditions. It has been shown previously that the flow fields are not qualitatively affected by the differences in the size or density of particles.[16] Therefore, convective mixing mechanism should still be present for particle mixtures. However, other mechanisms will also become effective, for example, percolation of small particles through gaps among large particles. For binary mixtures of particles of different sizes or densities, Zhou et al.[16] found that the forces acting on particles of different sizes or densities in the vertical direction differ, providing a driving to separate small and large or light and heavy particles. This mechanism can also be observed in this study concerning the same particle systems.

The binary mixtures considered in this work consist of particles of identical density but having a size ratio $r = 0.5$, with the large particles having a diameter of 8 mm, and the volume fraction α of the large particles is changed as 0.1, 0.5, and 0.9, while keeping the total particle volume fixed so that the mixture fills the space roughly up to the top of the vertical blades. The particles are loaded in the top–bottom arrangement, with the small particles being laid on top of the bed of large particles. The particle numbers of each type are listed in Table 1 as Cases 3–5. It should be noted that

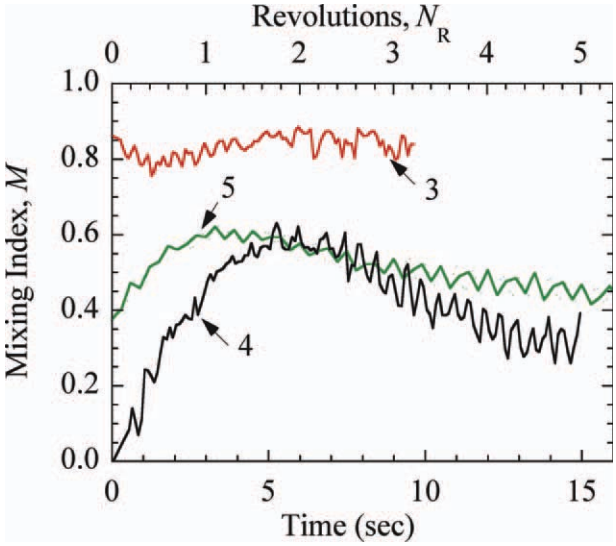

Figure 10. Macroscopic mixing index as a function of mixing time with the volume fraction of large particles as a parameter: curve 3, α = 0.1 (Case 3); curve 4, α = 0.5 (Case 4); and curve 5, α = 0.9 (Case 5).

[Color figure can be viewed in the online issue, which is available at wileyonlinelibrary.com.]

when α is increased from 0.1 to 0.9, the total number of particles in a mixture changes, because the total volume of particles in the present simulation is fixed. Therefore, of the three mixtures, Case 3 ($\alpha = 0.1$) and Case 4 ($\alpha = 0.5$) correspond to mixtures with predominantly small particles. Case 5 ($\alpha = 0.9$) corresponds to a mixture with predominantly large particles. Mixing in these cases will be examined at macroscopic and particle scales as described below.

General Behavior The states of the three mixtures are shown in Figure 9, in which (a) shows the states close to the start and (b) the states at the end of the mixing process. A segregated state can be observed in the snapshot of Case 3 in Figure 9b. Figure 9a shows the large particles deposited at the bottom initially. However, many of the large particles rising to the free surface of the bed get buried again by the small particles that flow down the steep heaps in front of the blades. Also one can observe that large particles are pushed toward the vessel wall. The snapshot for Case 4 in Figure 9b shows that small particles are collected at the bottom and in front of the blade. It also shows that mixing is still taking place as seen from both the large and small particles still flowing over the blade edge at steady-state. However, a majority of the large particles have risen above the small particles. By contrast, the snapshot (b) for Case 5 shows a clear segregation of the particles, with small ones being collected along the periphery of the bottom of the mixer and in front of the tip of the blades. The small particles at the blade tip build up, but fall over the blade into the bed bottom again entrained by the large particles. In any of the three cases above, particle jamming at the blade does not happen because there is no clearance between the moving blade and the vessel.

Macroscopic Index Figure 10 shows the macroscopic mixing index as a function of mixing time for the three cases. Mixtures for Cases 4 and 5 behave in a similar manner: M initially increases indicating mixing, but then decreases indicating demixing. Of the two mixtures, Case 4 has a larger total number of particles, and takes a longer time to reach the peak value. Demixing in Cases 4 and 5 follows different paths, with the final level of mixing for Case 4 reaching a lower value than for Case 5. For Case 5, the starting mixing index is about 0.4, which is somewhat larger as a result of small particles occupying only a single layer, resulting in many contacts with large particles. It can be seen from the animations generated that at the start of the shaft rotation, small particles in the heap in front of the blades mostly percolate through the matrix of large ones to the vessel bottom. Subsequently, small particles get collected in front of the blades by the sweeping action of the blades. The final value of M for Case 5 is about 0.43 after 34 s of mixing, which is not shown in the figure. The final value of M being close to the initial value, Case 5 ($\alpha = 0.9$) can be considered as being close to a complete segregation. By contrast, the final value of $M = 0.33$ for Case 4 is greater than the initial M value, which is nearly zero, and therefore, Case 4 ($\alpha = 0.5$) can be considered as partially mixed. Therefore, a judgment cannot be made about the state of the mixtures simply by assessing the final M values for Cases 4 and 5. It is well known that mean values and variances evaluated by sampling methods are hampered by variations in the sample size and number.[9,34] In Cases 4 and 5, the sample sizes will be different because when α is varied, the total volume of the bed changes; a sample is a number of particles fitting into a predefined space in the mixture (see Simulation Conditions section). Both the variations in the sample size and total particle number will affect the sample number. To account for these variations, we have used the weighted averaging method defined in Eqs. 4 and 5 to calculate the mixing index M.

M value for Case 3 ($\alpha = 0.1$) is large even from the very start of mixing. For this mixture, large particles are few in number. In a binary mixture of different sizes, large particles have been shown to rise to the free surface when being stirred in a bladed mixer due to the "buoyancy" forces exerted by small particles.[16] In fact, the observation from the animations confirm that large particles are rising to the free surface and some roll down the steep slopes of the particle heap in front of the blades toward the impeller shaft. Because of the convective motion, large particles also tend to move toward the vessel walls under the centrifugal forces acting on them. Although large particle rise above small particles, they are covered up again by the small ones, which are either flowing over the blade or along the free surface of the heap in front of the blades. This repetitive nature of the mixing process can be observed in the fluctuations of curve 3 in Figure 10. Conclusions at this point are that Case 3 is undergoing repetitions of mixing and demixing, Case 4 is partially segregated, and Case 5 is almost completely segregated.

Coordination Number It is known that coordination number of a binary mixture depends on the particle size ratio and volume fraction. Pinson et al.[35] have reported some experimental results on coordination numbers of binary mixtures of different particle sizes at static (packing) conditions. They observed that when the volume fraction of small

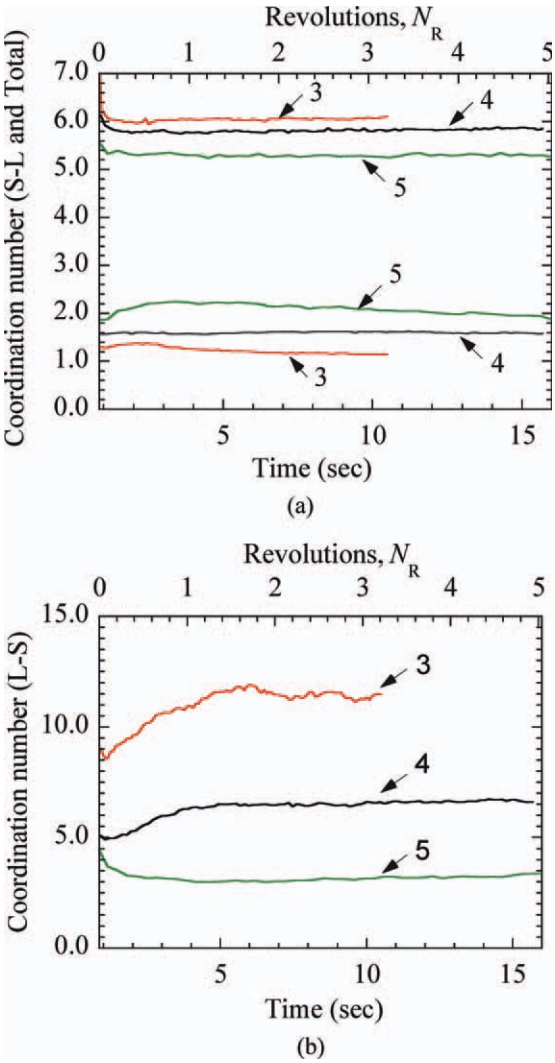

Figure 11. Coordination numbers based on (a) total contacts (top three curves) and S–L contacts (bottom three curves), (b) L–S contacts as a function of mixing time: curve 3, volume fraction $\alpha = 0.1$ (Case 3); curve 4, $\alpha = 0.5$ (Case 4); and curve 5, $\alpha = 0.9$ (Case 5).

[Color figure can be viewed in the online issue, which is available at wileyonlinelibrary.com.]

particles is increased, both the small-to-small (S–S) and large-to-small (L–S) particle contacts would increase, but the S–L and L–L contacts would decrease. For the present system, all the possible types of contact numbers for the three mixtures are shown in Figures 11a, b as a function of time. Figure 11a shows the average coordination number of the particle bed (top three curves) and the average S–L partial coordination number (referred to as S–L coordination number below, and a similar concept applied to L–S contacts) for the entire particle bed. Figure 11b shows the average L–S contacts (referred to as L–S coordination number below) for the entire bed.

Considering the coordination numbers, Case 3 ($\alpha = 0.1$) has the highest total coordination number of the three cases. The mixture in this case has a very large proportion of small particles when compared with the large ones (in a ratio of 72:1), and, therefore, the coordination number of the small particles will be the dominant factor in obtaining the average value. A comparison with Figure 4 shows that the total coordination number is almost identical to that of monosized particles. Case 4 ($\alpha = 0.5$) also has a larger proportion of small particles when compared with the large ones (in a ratio of 8:1) and, therefore, the coordination number of the small particles will still be the dominant one when obtaining an average value. The coordination number of a small particle cannot be as high as that for a uniform particle bed because of the presence of large particles. Therefore, the average coordination number will be lower than that for a uniform particle bed as confirmed from Figure 11a. Conversely, Case 5 ($\alpha = 0.9$) has the fewest total number of particles, and roughly equal numbers of large and small particles. Figure 9b shows that both types of particles are segregated into their own groups with some small particles still in contact with large particles. As a result, average coordination number for small particle bed will be close to that of a monosized particle bed, but the average for the large particle bed will be smaller than that for a monosized particle bed. Therefore, overall, the average coordination number for Case 5 will be lower than that for a monosized particle bed. Figure 11a shows that it has the lowest average coordination number of the three cases. The reason could be that the large particles, being above small particles as seen from Figure 11a, are dilated by blade motion reducing the coordination number further.

S–L coordination numbers are shown in Figure 11a. It shows that S–L contacts for Case 5 ($\alpha = 0.9$) are initially increasing gradually to reach a maximum, but returns to a value close to the initial value. Case 3 shows a similar behavior, but Case 4 does not show a significant change in S–L coordination number throughout mixing. Before discussing Case 4, consider Case 5. In Case 5, the small particles, if laid as a single layer, cover initially only about 83% of the (horizontal) cross-sectional area of the mixer. Therefore, mixing processes will increase the S–L contacts initially, because small particles, while percolating through large particle matrix make more contacts with large particles. However, when small particles start reaching the mixer bottom, S–L contacts begin to decrease because of the segregation of the two types of particles (Figure 10). As for Case 4, Figure 9 shows that most of the small and large particles have inverted their positions in the final state in comparison with the initial state. In the process, S–L contacts have remained constant from the very beginning of mixing. One possible explanation is as follows. Consider the mixing process from the start. When the blade is moved, S–L contacts will rise in the region in front of the blade, but small particles cannot penetrate the tighter large particle matrix there. However, when both types of particles flow over the blade, the large particle matrix becomes loose and small particles can penetrate to the bottom, thus reducing the S–L contacts. Therefore, when taking the average over the entire bed, S–L contacts would become roughly constant. Curves 3–5 in Figure 11a are in the ascending order of the number of large particles in the mixtures: the larger the number of large particles, the larger the S–L contacts. Based on above behaviors of S–L coordination number, one can conclude that Cases 3

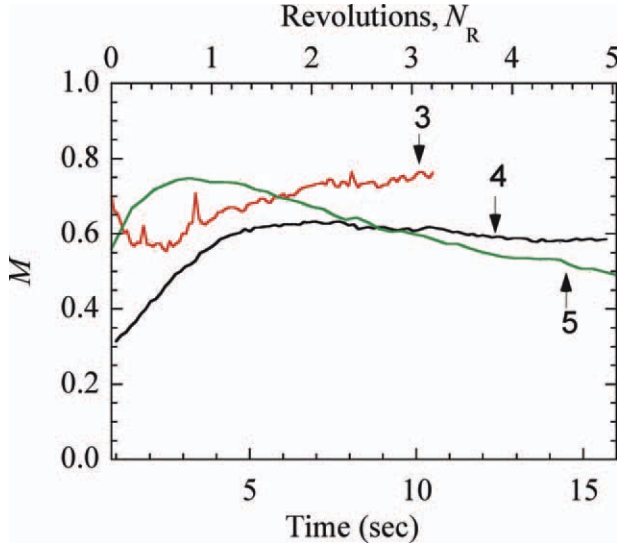

Figure 12. Particle-scale index as a function of mixing time for different volume fractions of large particles: curve 3, $\alpha = 0.1$ (Case 3); curve 4, $\alpha = 0.5$ (Case 4); and curve 5, $\alpha = 0.9$ (Case 5).

[Color figure can be viewed in the online issue, which is available at wileyonlinelibrary.com.]

and 5 are mixing initially but demix then. One cannot make a conclusion on Case 4 whether it is mixing or not.

The S–L coordination number for Case 5 at the steady-state is about 1.92, which is in reasonable agreement with the measurements by Pinson et al.,[35] who predicts a value of about 2.5 at $\alpha = 0.9$ for particles under packed or static conditions. It should be noted that the comparison between simulated and measured results here has to be qualitative but not quantitative, because the beds were generated under different conditions. The bed in this work is dynamic and non-uniform in structure. In fact, the snapshot of Case 5 in Figure 9b shows that small particles are mostly segregated from the large ones. This segregation causes a reduction in the S–L coordination number in the simulations when compared with the experiments. For the same reasons, differences between simulated and measured results can also be observed in other cases. For example, Cases 3 and 4 have S–L coordination numbers of 1.15 and 1.6, respectively, higher than the actual measurements, which are 0.22 ($\alpha = 0.1$) and 1.12 ($\alpha = 0.5$).

L–S coordination numbers are shown in Figure 11b. Both Case 3 ($\alpha = 0.1$) and Case 4 ($\alpha = 0.5$) show initial increases and then reach steady-state values. However, Case 5 ($\alpha = 0.9$) shows a decrease from the very beginning of mixing and then reaches a steady-state value. In the three cases, large particles are at the bottom of the vessel initially, and, hence, the L–S contacts are limited to the interface contacts only. However, with the start of mixing, L–S contacts should increase in Cases 3 and 4 because of the dispersion of the large particles in the predominantly small particle matrix. On the other hand, L–S contacts will decrease in Case 5 because of the dispersion of small particles in the large particle matrix. Case 3 shows fluctuations at steady-state, which is a sign of both mixing and demixing occurring.

A description follows regarding the relative magnitudes of L–S coordination numbers and a comparison with measurements. Cases 3 and 4 both have large proportions of small particles, the proportions of the large-to-small particles of Cases 3–5 are being 1:72, 1:8, and 1:0.9, respectively (Table 1). The larger the proportion of the small-to-large particles, the larger the L–S coordination number. Therefore, steady-state values of L–S coordination numbers can be arranged naturally in the descending order as Cases 3–5, which is true as seen from Figure 11b. As for the actual values, the steady-state value for Case 3 is 11.4, which is in good agreement with the measurements by Pinson et al.,[35] who predicted value of 13.5. Case 5 has a steady-state value of about 3.2, which is in good agreement with their predicted value of about 3.6 for a binary mixture of 1:2 size ratio mixed at $\alpha = 0.9$. On the other hand, Case 4 has a steady-state value of 6.6 as against their predicted value of 10.6. As discussed above, the measurements are for packed particles in a mixed state, and the present simulations are for dynamic particles in a partially segregated state. In a dynamic and segregated bed, a large particle may have fewer contacts with small ones leading to a smaller L–S coordination number. Moreover, bed dilation under dynamic conditions also

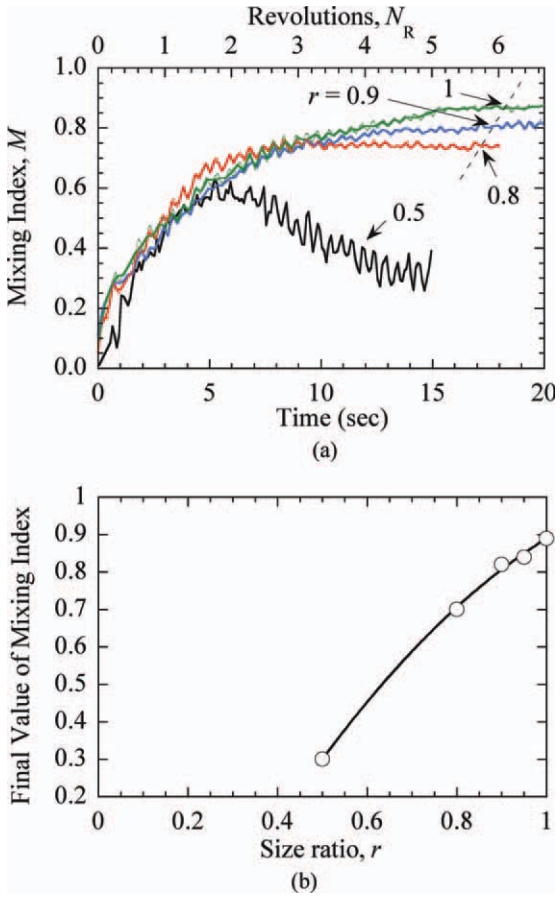

Figure 13. Effect of particle size ratio on macroscopic mixing.

(a) Mixing index M as a function of time and (b) steady-state values of M as a function of the size ratio r of small-to-large particles expressed as a fraction. [Color figure can be viewed in the online issue, which is available at wileyonlinelibrary.com.]

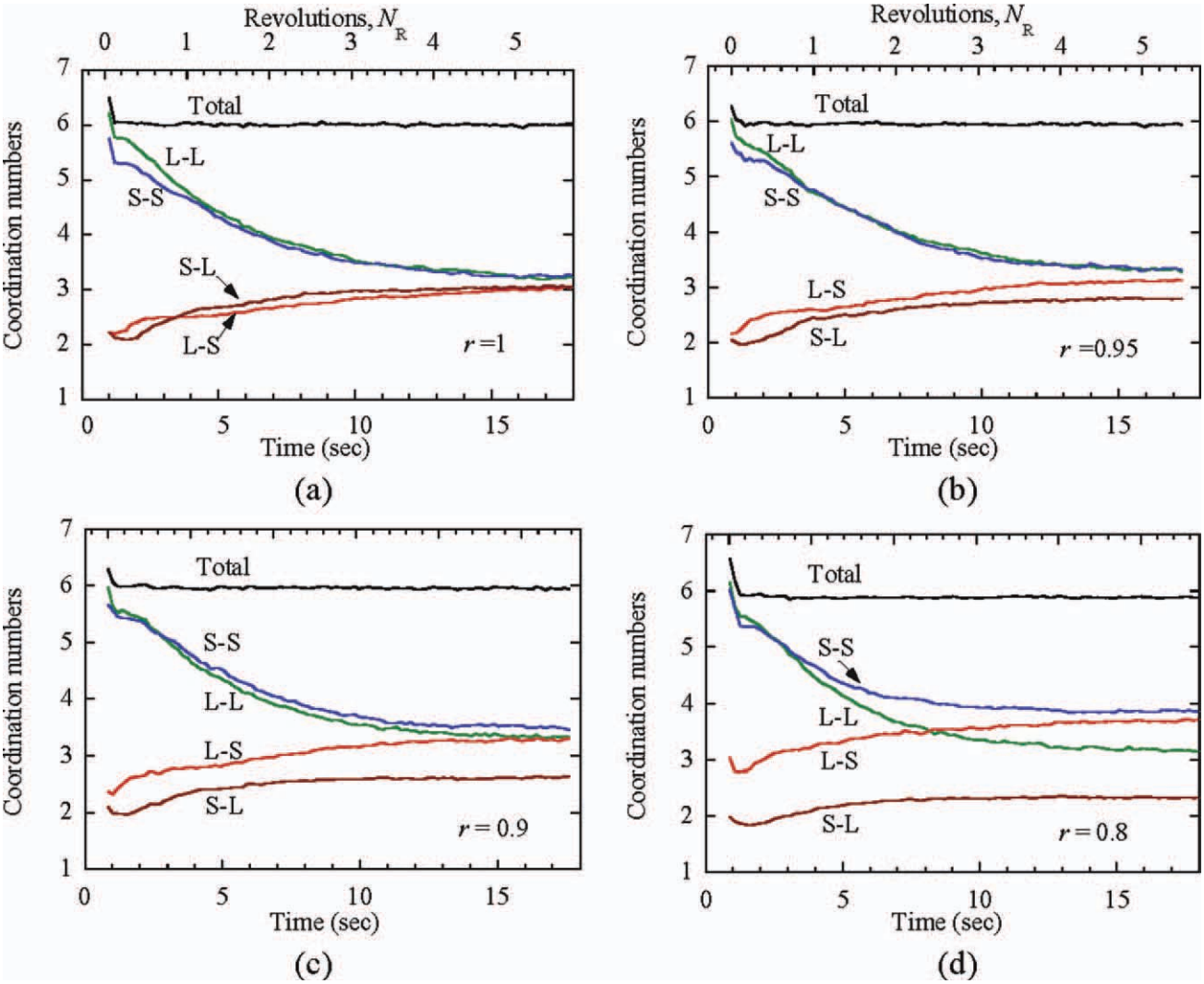

Figure 14. Coordination numbers as a function of time when diameter ratio r is changed with $\alpha = 0.5$: (a) $r = 1$, (b) $r = 0.95$, (c) $r = 0.9$, and (d) $r = 0.8$.

The letters S and L represent small and large particles, respectively; for $r = 1$, L and S represent simply particles of different colors; a contact type is represented by a combination of the letters; and loading is the top and bottom arrangement with S laid on the top of L. [Color figure can be viewed in the online issue, which is available at wileyonlinelibrary.com.]

reduces the contact numbers. Because of these factors, Case 4 ($\alpha = 0.5$), which is the intermediate one of the three cases, shows a larger difference. Nevertheless, the coordination numbers generated from the simulations are in good qualitative agreement with the measurements by Pinson et al.[35]

Based on S–L and L–S coordination numbers, Case 5 can be considered as corresponding to a mixture, which initially mixes and then demixes. Case 4 corresponds to a mixture that mixes initially and reaches a steady-state. Case 3 corresponds to a mixture that mixes and segregates continuously at steady-state. In general, it is hard to decide the state of a mixture from coordination number information alone.

Above analyses of coordination numbers show that L–S coordination number is sensitive to changes in the volume fraction, but S–L coordination number is not sensitive enough. However, the importance of L–S coordination number cannot be ignored because L–S coordination number has not been able to show evidence of demixing or segregation. To detect these conditions with certainty, consideration of S–S and L–L coordination numbers will also be useful as will be done in the sections to follow.

Particle-Scale Index Figure 12 shows the particle-scale index M for the three mixtures. M values for Case 3 show an initial decrease, to be followed by an increase and then to reach a steady state. Case 4 shows an initial increase in M, then reaching a peak value and finally reaching steady state. The steady-state value of Case 4 is lower than that of Case 3. Case 5 also shows an initial increase in M, then reaching a peak value and finally reaching a steady-state M value of about 0.4 at 34 s, which is not shown in the figure. The differences of M at the start of mixing are caused by the differences between the actual initial value of $S_t^2 = (S_{t=0})^2$ and S_0^2 $(=\sigma_0^2)$ which is a fixed value. For example, in Case 3, $(S_{t=0})^2$ is smaller in comparison with S_0^2 indicating an initial mixed state, because the large particles at the vessel bottom are dispersed among the small particles

(Figure 9a). Conversely, $(S_{t=0})^2$ for Case 4 is closer to σ_0^2, because the bulk of the particles are clearly segregated (Figure 9a). In Case 5, $(S_{t=0})^2$ is larger in comparison with σ_0^2 because small particles few in number are resting on top of the large particles indicating an initial mixed state (Figure 9a).

At the end of simulation, Case 3 has a larger M value than Case 4, which in turn is having a larger M value than Case 5. Therefore, the mixture quality can be ranked in the ascending order of Cases 5, 4, and 3. In addition, Cases 3 and 4 each reach a better mixed state at the end of the simulations than they are each at the start of mixing, although they do not approach unity. Conversely, Case 5 indicates a worse mixing state than it is at the start of the mixing. Therefore, it can be argued that Cases 3 and 4 produce partially mixed states and that Case 5 produces a segregated state. These observations are consistent with the general behavior of particles shown in the snapshots of Figure 9.

There are subtle differences in the mixing index at the particle and macro scales. For example, the particle-scale index for Case 4 shows only a cross-over point with that of Case 5 (Figure 12), whereas the macroscale index shows a merger of the two curves over a long period of time (Figure 10). In addition, the particle-scale index displays a greater sensitivity to changes in the volume fraction than the macroscale index (Figures 10 and 12). This sensitivity is associated with the particle-scale index being linked to the mixture structure as well as not being susceptible to the two uncertainties, the sample size and number. Therefore, the particle-scale index M is a better method to describe structural changes associated with mixing and segregation. Coordination number variations, on the other hand, are very useful for gaining information on the mixing and segregation mechanisms, but that information alone is not enough to gauge the quality of a mixture.

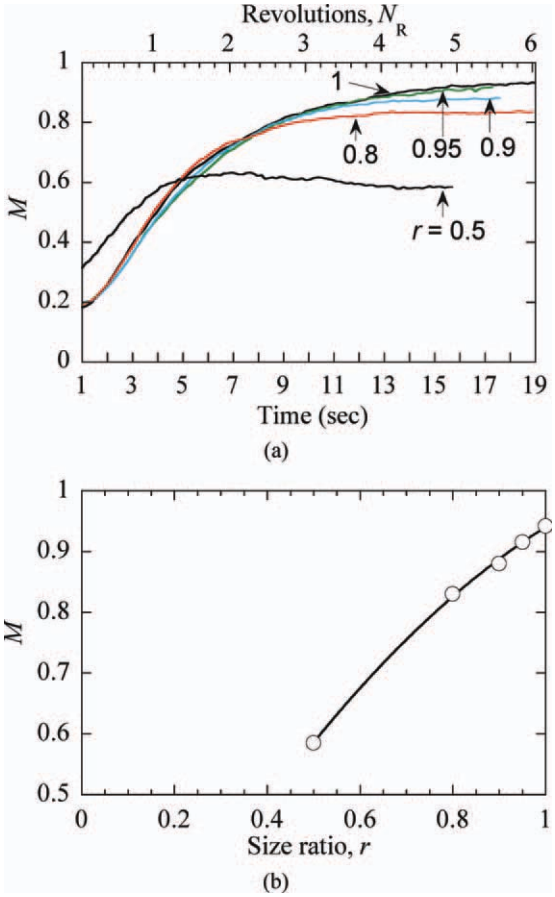

Figure 15. Effect of particle size ratio on particle-scale mixing.

(a) Mixing index as a function of time and (b) steady-state value of index as a function of size ratio of small-to-large particles expressed as a fraction. [Color figure can be viewed in the online issue, which is available at wileyonlinelibrary.com.]

Mixing of binary particles: effect of size ratio

The effect of the size ratio of binary particles is now examined. The size ratios r used are 0.5, 0.8, 0.9, 0.95, and 1, which correspond to Cases 4, 8, 7, 6, and 9, respectively, listed in Table 1. The volume fraction α of large particles is fixed at $\alpha = 0.5$ throughout. The particles are loaded initially in the T–B loading arrangement with the small particles laid on top of the large particles. Simulations have been limited to $r = 0.5$ and above because, for $r < 0.5$ the number of small particles and the computational time are increased too much.

Macroscopic Index Figure 13a shows the macroscopic index as a function of time for Cases 6–8, in which the diameter of the large particle is kept constant while that of the other type is reduced. Also included are the mixing indexes for Case 1 ($r = 1$) and that of Case 4 ($r = 0.5$) already shown. The value of the mixing index attained at the end of each simulation is shown in Figure 13a as a function of the small-to-large size ratio r.

Although all the results show similar increases in M for all size ratios, Case 4 ($r = 0.5$) shows a maximum at about 5 s, marking the end of mixing. Demixing then develops and a steady state value, which is far inferior to that of the monosized case, arises. Case 8 ($r = 0.8$) shows related behavior. The other cases show a gradual deterioration of mixing when compared with the monosized case, with the decrease of size ratio.

Figure 13b shows the values of macroscopic index M at the end of each simulation as a function of the size ratio. It shows that the steady-state value of M varies monotonically with the size ratio, the larger the reduction in size ratio, the larger the deterioration of mixture quality. Porion et al.[36] reports that segregation in a blender occurs due to the particle size difference when the size difference is about 10% ($r = 0.9$), when roughly equal volumes of materials are mixed in the blender at 22 rpm. They quantified the segregation by using the segregation index I (Eq. 3). This work supports the fact that a significant change (10%) in the macroscopic index occurs when the diameter difference is about 10% as seen from Figure 13b.

Coordination Number The coordination numbers are obtained for the four types of contacts when the mixing progresses: the four types are L–L, S–S, L–S, and S–L, where the letters S and L represent small and large particles, respectively, and the first letter shows the core

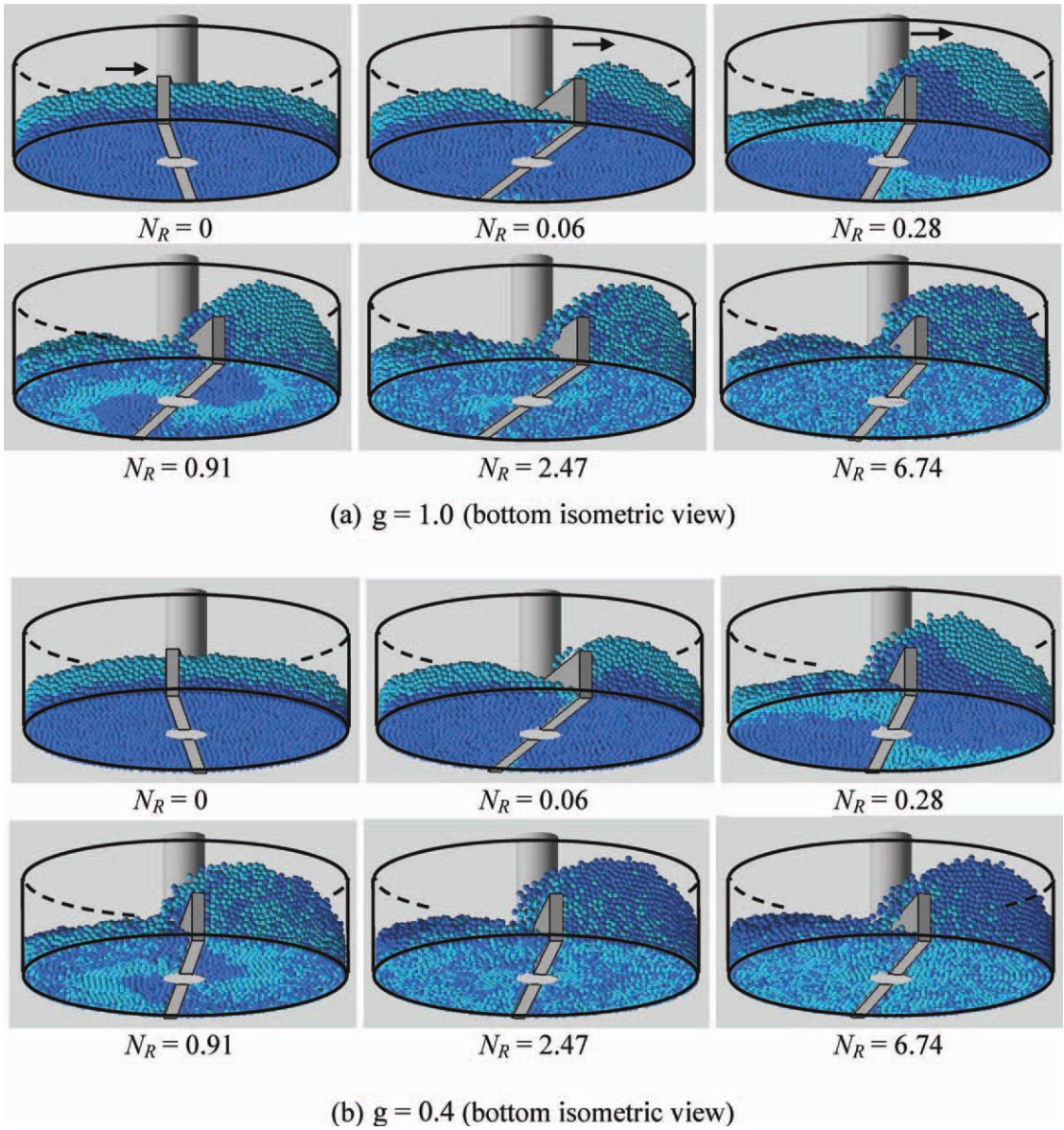

Figure 16. Mixing states of binary mixtures of different density ratios at different shaft revolutions N_R.

Arrows show the direction of motion of the front blade. (a) $\gamma = 1.0$ (bottom isometric view) and (b) $\gamma = 0.4$ (bottom isometric view). [Color figure can be viewed in the online issue, which is available at wileyonlinelibrary.com.]

particle in particle contacts (Figure 1). Considering the larger particle to be the target particle in the analysis, we obtain instantaneous frequency distribution for each type of particle contacts at the time intervals of 0.01 s from the start of the mixing until the steady state is reached. Next, the mean value for each distribution is obtained at each instant. Figures 14a–d show the mean coordination number for each type of contacts as a function of time for Cases 6–9 in Table 1.

In Figure 14a, S–L and L–S coordination number curves are seen to be separated at the beginning of mixing, but converge to a single value at the steady-state. Similar trends are observed in Figure 4b with a blade gap of 1.5 d, but there the two curves converge earlier than in Figure 14a. This indicates that the blade clearance at the vessel bottom improves mixing.

From a solid-angle analysis, the maximum numbers of small particles that can be arranged around a large core particle are: 14, 15, 16, 20, and 34 for a size ratio, r of 1, 0.95, 0.9, 0.8, and 0.5, respectively. Therefore, one can expect that L–S contacts should increase with the decrease of size ratio r because the population of S is a majority. Conversely, S–L contacts should decrease because the population of L becomes a minority. Figures 14a–d confirm this behavior. In fact, at the steady-state, L–S contacts have increased by about the same amount as S–L contacts have decreased with respect to the case of $r = 1$. This change alone can not be considered an indication of segregation, because it is a natural outcome of the increase in the S particle population as a result of the reduction in the size ratio (Table 1). Increasing the S particle population should increase S–S contacts,

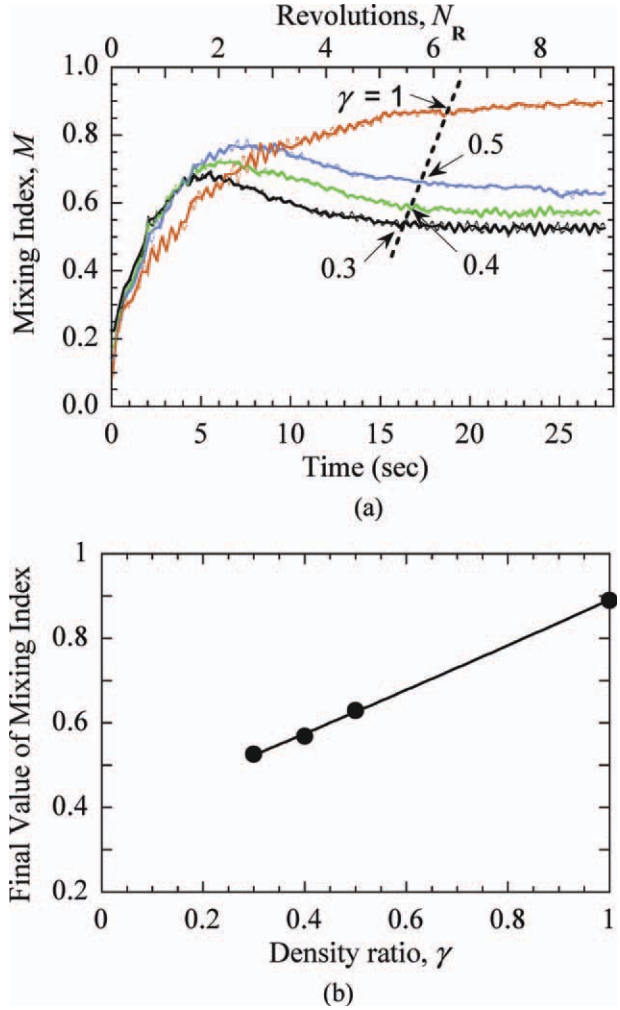

Figure 17. Effect of density ratio in terms of macroscopic mixing index.

(a) Mixing index (M) as function of time and (b) steady-state values of M as a function of γ, which is the light-to-heavy density ratio. [Color figure can be viewed in the online issue, which is available at wileyonlinelibrary.com.]

which is true as seen from the figure. Conversely, the increasing in the S particle population should have decreased L–L contacts, which is not true as seen from the figure. In fact, L–L contacts remain more or less the same as in the case of $r = 1$, despite the increase in the small particle population. If segregation occurs in the large particle population, L–L contacts should have increased, which is not true either. Therefore, it can be argued that the large particles are mixing with small particles, but some small particles are segregating as seen from the increase of S–S contacts, creating a partially mixed state in the mixture when r is reduced.

Particle-Scale Index To find the particle-scale index M as a function of time, the procedure described in Particle-Scale Index section is followed. Here, a larger particle is considered as the target type of particle in obtaining particle fractions, and M values at time intervals of 0.01 s are obtained from the start of mixing until the steady state is reached.

Figure 15a shows M as a function of time for the size ratios, $r = 0.80$, 0.90, 0.95, and 1. The figure also shows the results of M for Case 4 ($r = 0.5$). Note that Case 4 has an initial mixing index different from the other four cases. M deviates progressively from the monosized behavior when the size ratio is reduced. Figure 15b shows M values at the end of the simulations as a function of size ratio. It shows that the steady state value of M for $r = 0.9$ is about 92% of that of $r = 1$. Namely, a diameter difference of 10% causes an 8% reduction in the mixing index at $\alpha = 0.5$. Therefore, particle-scale index shows a similar behavior to the macroscopic index above.

A comparison of Figures 15a and 13a shows that the fluctuations of the particle-scale index with time are very small when compared with the fluctuations in the macroscopic index. The smaller fluctuations result from the large number of samples being used in the microscopic analysis. In addition, it also shows that the maximum point for $r = 0.5$ occurs at around 7 s in the macroscopic index, but such a point in the particle-scale index occurs between 5 and 7 s. On the other hand, the transition in M from the peak mixed state to the segregated state is more visible at the macroscale than at the particle scale for $r = 0.5$. Although there are slight differences between the macroscopic and particle-scale indexes, they both predict similar behavior for the size segregation in binary mixtures.

Mixing of binary particles: effect of particle density

Segregation will also occur for particles of different densities. Zhou et al.[16] investigated this phenomenon by DEM simulations for particles having 500 and 2500 kg/m^3 densities, loaded in the side-by-side arrangement at a rotation speed of 20 rpm. Their results suggest that light particles remain mainly at the top and outer regions of the bed, whereas heavy particles will sink to the mixer bottom. There are large vertical forces acting on light particles, leading to segregation. Here, segregation studies are conducted to clarify the effect of a top–bottom loading arrangement. Case 9 in Table 1 lists the particle and mixer details. To investigate

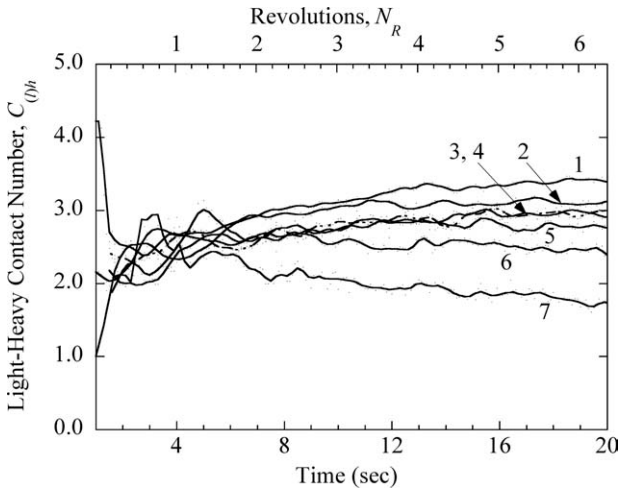

Figure 18. Average contact number $C_{(l)h}$ of light (l) particles with heavy (h) ones as a function of time for $\gamma = 0.4$.

Sections 1 to 7 are numbered sequentially from the bottom to top.

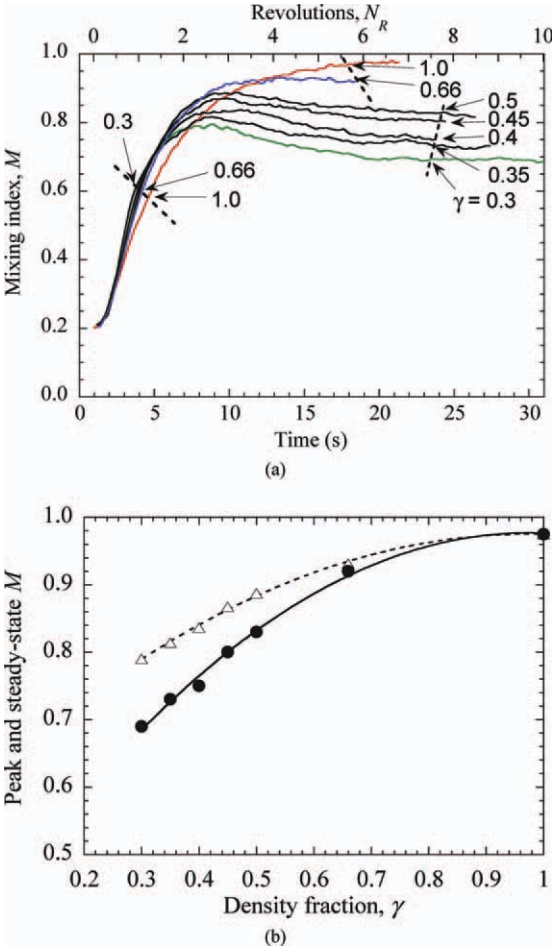

Figure 19. Effect of density ratio on mixing based on the particle-scale index.

(a) Variation of M as a function of time and (b) maximum and stead-state values of M as a function of γ, Δ represents peak values and $\bullet$ represents steady-state values. [Color figure can be viewed in the online issue, which is available at wileyonlinelibrary.com.]

the effect of density difference, the density of heavy particles is kept constant at 2500 kg/m^3, whereas that of the lighter particles is reduced to produce the light-to-heavy density ratios γ of 1, 0.66, 0.5, 0.45, 0.4, 0.35, and 0.3.

General Behavior Figure 16a shows the bottom isometric images (namely, viewed at an angle to the bottom of the vessel) of mixing states of the top–bottom loaded particles that differ only in color at several blade revolutions N_R from the start of mixing. Figure 16b shows the images of mixing states at the corresponding N_R values for the top–bottom loaded particles when $\gamma = 0.4$. When a blade rotates from its initial position at $N_R = 0$ in counterclockwise direction (in the direction of the arrow), the wall of particles behind the blade collapses to fill up the void space momentarily left behind by the advancing blade as seen from figures at $N_R = 0.06$. Particles at the top of the particle bed move into this space from two directions: along the slope behind the blade and from over the top of the blade as seen from the images at $N_R = 0.06$ and 0.28. Up to $N_R = 0.28$, mixing progresses in both the systems in a similar manner. The particles that initially sank to the bottom, form an inverted S-shaped image at the bottom as seen from the images at N_R =0.91 in the either case.

The inverted "S-shape" for $\gamma = 0.4$ contains mostly heavy particles, because heavy particles were initially loaded at the top of the bed. It is also seen to be wider than that for $\gamma = 1$. The images shows that the heavy particles in the heap in front of the blades have moved more toward the vessel bottom in comparison with the case of $\gamma = 1$. With the advancement of N_R, the inverted S-shape diffuses. At $N_R = 2.47$, there are more heavy particles at the bottom and in the peripheral region of the vessel than in the respective places of the corresponding image for $\gamma = 1$. The same description applies to the advanced state of $N_R = 6.74$. These images show that sinking of the heavy particles mostly occur in the peripheral region of the vessel, where the particles move faster, thus with an increased likelihood of segregation due to such reasons as increased momentum and porosity.

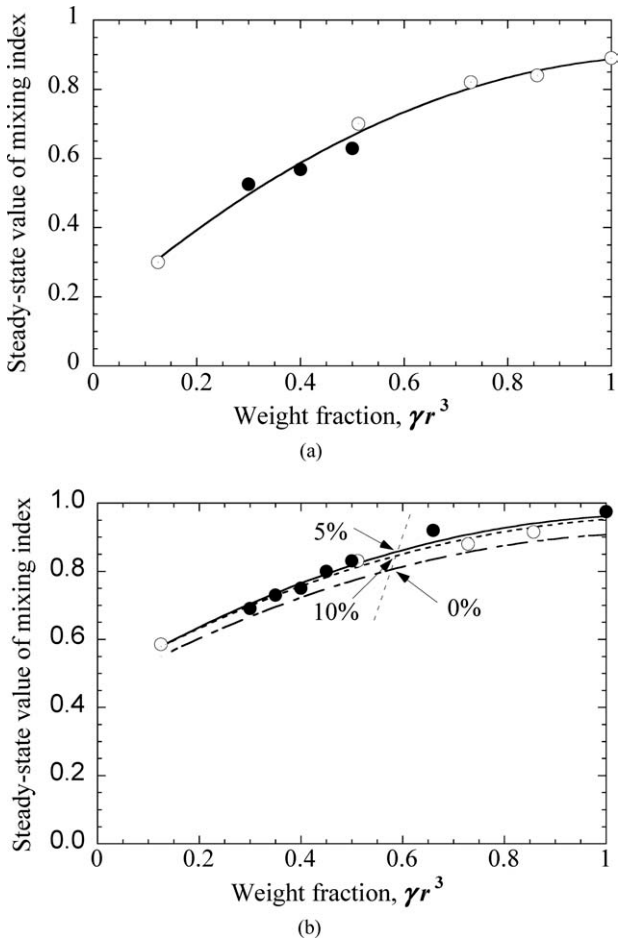

Figure 20. Effects of the size and density differences expressed in terms of weight fraction γr^3, where γ is density fraction and r the size ratio.

(a) At macroscopic scale, (b) at the particle scale, ○ represents data with size-ratio as variable, ● data with density fraction as variable, and trendlines in (b) show the particle-scale index evaluated at gap sizes of 0%, 5% and 10% of particle diameter.

Macroscopic Index Figure 17 shows the effect of density difference when the macroscopic mixing index M is used to analyze the mixing of the binary particles with different densities. The curve $\gamma = 1$ shows the mixing index for uniform particles, and it gradually increases and approaches an asymptotic value indicating mixing. Contrarily, with $\gamma < 1$, a curve shows a maximum, indicating particle segregation in the mixing operation past the point of greatest mixedness. The maximum value in M decreases with a decrease in γ. The steady-state value of M is shown in Figure 17b as a function of γ, and it also decreases with a decrease in γ.

Coordination Number Figure 18 shows average contact number $C_{(l)h}$ of a light particle (l) with heavy particles (h) as a function of time with $\gamma = 0.4$ in several slices sectioned horizontally, the thickness of each slice being 10 mm. $C_{(l)h}$ remains roughly uniform in the axial direction in the time interval between 3 s and 6 s. This indicates that a mixed state was initially developing. However, after this period, $C_{(l)h}$ shows stratification of particles as indicated by curves 1–7, heavy particles being more concentrated at the bottom than at the top, respectively.

Particle-Scale Index Figure 19a shows the particle-scale index M as a function of time. For comparison, data for uniform particles (Case 9) is also shown in the figure by $\gamma = 1$ line. For these particles, the index is close to 1 after about 6 revolutions. When $\gamma < 1$, M shows an initial increase with time but reaches a maximum and then a steady-state value. These effects are enhanced further by a decrease in γ (Figure 19b). Such a maximum is an indication that particles of different densities are segregating; however, complete segregation does not occur because steady-state M is quite large indicating a partially mixed state. Figure 19 also shows that there is an optimum number of shaft revolutions to attain the best mixed state, which varies between 2 and 4 revolutions depending on γ. There is also an increase in the initial rate of mixing when γ is reduced, with $\gamma = 0.3$ showing the highest rate and $\gamma = 1$ the lowest. Therefore, the particle-scale index has been able to detect the segregation of particles that brings about structural changes to the mixture. A comparison of Figure 19 with Figure 17 shows that the mixing indexes at the macroscopic and particle scales behave in a similar manner.

Mixing studies were also conducted for the case of S–S rotated loading with $\gamma = 0.5$. As observed with the case of monosized particles (Figure 8), this loading pattern caused mixing to be delayed considerably. M increased monotonically from an initial value of 0, with mixing time, but the rate of mixing decreased gradually, for example, from a rate of 0.025 s^{-1} at 10 s, where $M = 0.25$ to a rate of 0.017 s^{-1} at 61.8 s, where $M = 0.62$. No maximum value in M was observed in this period. Therefore, one can deduce that the maximum value in the mixing index is peculiar to top–bottom loading arrangement.

Comparison of Segregation due to Size and Density Differences A binary mixture of particles being mixed in a cylindrical mixer segregates due to the effect of a driving force that reflects the competition between the two vertical forces, weight, and buoyancy force on a particle.[16] This driving force is affected by many variables, among which are the size ratio and density ratio as discussed above. Similar phenomena can be found in the case of a rotating drum.[37] It would be of interest to quantify the equivalence between the two variables. Here, we compare the previous steady-state results of M for particle size and density differences (Figures 13b, 15b, 19b, and 17b) on the basis of weight fraction w_r ($= \gamma r^3$) of particles as shown in Figures 20a, b at macroscopic and particle scales, respectively. The figures show that effects of particle size and density differences can be represented by a single curve at the macroscopic and particle scales. Note that r^3 represents the volume ratio between particles. The existence of such a unique curve indicates that the driving force for segregation is caused by the weight difference between the two types of particles in the mixture. Different mixtures and/or different types of mixers may give different M–w_r relationships. Nonetheless, if confirmed to hold generally, this finding can lead to significant simplification in the modeling of the mixing of particles. Notably, as also shown in Figure 20b, the results are not sensitive to different gap sizes, which further confirms the effectiveness of the particle-scale index as discussed above.

Conclusions

DEM simulations were carried out to investigate the quality of mixing of noncohesive particles in a vertically-shafted bladed mixer both at the macroscopic and particle scales. The quality of mixing was examined for different types of mixtures in three different ways: a macroscopic mixing index, coordination numbers, and a particle-scale index. The followings are the conclusions regarding the general mixing behavior and mixing characterization methods investigated.

For uniform particles, different loading patterns produce different mixing rates, the side-by-side arrangement being the fastest of the three loading arrangements tested. A blade clearance at the vessel bottom is proven to be effective for further increasing the mixing rate. Neither the initial loading arrangement nor blade clearance affects the final mixing state according to the particle-scale index. The final value is close to 1 according to both the macroscopic and particle-scale indexes and, therefore, the two blade impeller can successful randomize uniform particles in the mixer.

For binary mixtures, particle segregation is caused by differences in particle size and density. By changing the volume fraction of large particles in a binary-sized particle mixture, mixing behavior can be significantly changed, with a smaller volume fraction producing a mixed state whereas a larger one producing a segregated state. Further, a reduction in the small-to-large diameter ratio causes the mixing to deteriorate gradually. A reduction in the light-to-heavy density ratio in a monosized binary mixture results in a similar mixing behavior. The similarity between the size and density effects can be further proven by the fact that both effects could be unified, using the particle weight ratio. The generality of this approach should be investigated in future studies.

Powder mixing can be analyzed at different length scales: contact point, particle scale, and sampling cell scale. The results suggest that coordination number variations are useful to identify the mechanisms of mixing and demixing. However, the coordination number results are not straightforward and need to be properly interpreted for this purpose. The particle-scale index proposed in this work can identify the

structural changes in association with mixing or segregation behavior. The case studies presented demonstrate that the index is more superior to the conventional macroscopic index, which heavily depends on the sampling method and may even be system-dependent. Obtained directly from the particle-scale data generated by DEM simulations, the index can link the structural information to mixing quality without the hassle of finding a suitable sampling technique.

Acknowledgments

This work was supported by Australian Research Council (ARC).

Notation

$Cn_{B(W)}$ = number of B-type contacts for the core particle i of W-type
$Cn_{B(B)}$ = number of B-type contacts for the B-type particle i
Cn_i = total coordination number of the particle i
d = diameter of particles in monosized mixture, (m)
d_1, d_2 = diameters of particles of the two types of particles in a binary mixture
G = gap or clearance of the blade at the bottom, (m)
I = segregation index
M = degree of mixing in Eq. 1 or macroscopic mixing index defined in Eq. 2 or particle-scale index in Eq. 11
N = particle number in the mixture for analysis of particle-scale mixing index
N_0 = number of samples drawn from the mixture for the analysis of macroscopic mixing index, which can vary with time
N_1, N_2 = number of particles of the two types of particles in a binary mixture
n = sample size
p = mixing ratio or the overall particle number fraction of the target type particles
p_i = particle fraction of a target type particle in the neighborhood of particle i
$\overline{p}_t$ = average value of p_i at time t for the entire mixture
S_0 = standard deviation of particle-scale particle fraction at the fully segregated state for particles mixed with a particle fraction of p
S_R = standard deviation of particle-scale particle fraction at the fully mixed state for uniform-sized particles mixed with a particle fraction of p
S_t = standard deviation of p_i with respect to $\overline{p}_t$ defined in Eq. 13
V_1, V_2 = total particle volumes of the two types of particles in a binary mixture
V_i, V_T = volume of particles in sample i and total volume of particles in a mixture, respectively, (m^3)
w_i = weighting used in averaging of sample related values
x_i = number fraction of particles of a target type in the macroscopic sample i
$\overline{x}_t$ = instantaneous average value of x_i at time t for all the samples N_0
α = volume fraction of the target type particles in a binary mixture
σ_0 = standard deviation for fully segregated state
σ_r = standard deviation of fully mixed state for uniform-sized particles of particle fraction of p and sample size of n
σ_t = standard deviation of x_i at time t with respect to $\overline{x}_t$
γ = density ratio

Literature Cited

1. Prescott JK, Hossfeld RJ. Maintaining product uniformity and uninterrupted flow to direct compression tablet presses. *Pharmaceut Technol*. 1994;18:99–114.
2. Kangwantrakool S, Shinohara K. New design of microstructure of WC-Co/TiC-Al2O3 composite materials by mechanical coating of particles. *J Jpn Soc Powder Powder Metall*. 2002;49:56–60.
3. Saberian M, Segonne Y, Briens C, Bousquet J, Chabagno JM, Denizart O. Blending of polymers in high speed, vertical mixers: development of a thermal tracer measurement procedure. *Powder Technol*. 2002;123:25–32.
4. Yang B, Sato M, Kuriyama T, Inoue T. Improvement of a gram-scale mixer for polymer blending. *J Appl Polym Sci*. 2006;99:1–5.
5. Liang H, Ueno A, Shinohara K. UV protection effectiveness of plastic particles coated with Titanium Dioxide by rotational impact blending. *Chem Eng Res Des*. 2000;78:49–54.
6. Poux M, Fayolle P, Bertrand J, Bridfoux D, Bousquet J. Powder mixing: some practical rules applied to agitated systems. *Powder Technol*. 1991;68:213–234.
7. Missiaen JM, Thomas G. Homogeneity characterization of binary grain mixtures using a variance analysis of two-dimensional numerical fractions. *J Phys Condens Matter*. 1995;7:2937–2937.
8. Akao Y, Kunisawa H, Fan LT, Lai FS, Wang RH. Degree of mixedness and contact number. *Powder Technol*. 1976;15:267–277.
9. Akao Y, Shindo H, Yagi N, Fan LT, Wang RH, Lai FS. Estimation of mixing index and contact number by spot sampling. *Powder Technol*. 1976;15:207–214.
10. Lacey PMC. Developments in the theory of particle mixing. *J Appl Chem*. 1954;4:257–268.
11. Siiriä S, Yliruusi J. Determining a value for mixing: mixing degree. *Powder Technol*. 2009;196:309–317.
12. Stewart RL, Bridgwater J, Zhou YC, Yu AB. Simulated and measured flow of granules in a bladed mixer—a detailed comparison. *Chem Eng Sci*. 2001;56:5457–5471.
13. Hassanpour A, Tan H, Bayly A, Gopalkrishnan P, Ng B, Ghadiri M. Analysis of particle motion in a paddle mixer using discrete element method (DEM). *Powder Technol*. 2011;206:189–194.
14. Zhu HP, Zhou ZY, Yang RY, Yu AB. Discrete particle simulation of particulate systems: a review of major applications and findings. *Chem Eng Sci*. 2008;63:5728–5770.
15. Zhou YC, Yu AB, Stewart RL, Bridgwater J. Microdynamic analysis of the particle flow in a cylindrical bladed mixer. *Chem Eng Sci*. 2004;59:1343–1364.
16. Zhou YC, Yu AB, Bridgwater J. Segregation of binary mixture of particles in a bladed mixer. *J Chem Technol Biotechnol*. 2003;78:187–193.
17. Chandratilleke GR, Yu AB, Stewart RL, Bridgwater J. Effects of blade rake angle and gap on particle mixing in a cylindrical mixer. *Powder Technol*. 2009;193:303–311.
18. Chandratilleke GR, Zhou YC, Yu AB, Bridgwater J. Effect of blade speed on granular flow and mixing in a cylindrical mixer. *Ind Eng Chem Res*. 2010;49:5467–5478.
19. Remy B, Glasser BJ, Khinast JG. The effect of mixer properties and fill level on granular flow in a bladed mixer. *AIChE J*. 2010;56:336–353.
20. Remy B, Canty TM, Khinast JG, Glasser BJ. Experiments and simulations of cohesionless particles with varying roughness in a bladed mixer. *Chem Eng Sci*. 2010;65:4557–4571.
21. Radeke CA, Glasser BJ, Khinast JG. Large-scale mixer simulations using massively parallel GPU architectures. *Chem Eng Sci*. 2010;65:6435–6442.
22. Fan LT, Chen SJ, Watson CA. Solids mixing: annual review. *Ind Eng Chem*. 1970;62:53–69.
23. Fan LT, Too JR, Rubinson RM, Lai FS. Studies on multicomponent solids mixing and mixtures. Part III. Mixing indices. *Powder Technol*. 1979;24:73–89.
24. Danckwerts PV. The definition and measurement of some characteristics of mixtures. *Appl Sci Res*. 1952;3:279–296.
25. Yamane K. Discrete-element method application to mixing and segregation model in industrial blending system. *J Mater Res*. 2004;19:623–627.
26. Dodds JA. The porosity and contact points in multicomponent random sphere packings calculated by a simple statistical geometric model. *J Colloid Interface Sci*. 1980;77:317–327.
27. Carter F. Quantifying the concept of coordination number. *Acta Crystallogr B*. 1978;34:2962–2966.
28. Shindo H, Yoshikawa T, Akao Y, Fan LT, Lai FS. Estimation of mixing index and contact number by spot sampling of a mixture in an incompletely mixed state. *Powder Technol*. 1978;21:105–111.

29. Zhu HP, Zhou ZY, Yang RY, Yu AB. Discrete particle simulation of particulate systems: theoretical developments. *Chem Eng Sci*. 2007;62:3378–3396.
30. Massol-Chaudeur S, Berthiaux H, Dodds JA. Experimental study of the mixing kinetics of binary pharmaceutical powder mixtures in a laboratory hoop mixer. *Chem Eng Sci*. 2002;57: 4053–4065.
31. Hogg R. Mixing and segregation in powders: evaluation, mechanisms and processes. *KONA Powder Part J*. 2009;27:3–17.
32. Radl S, Kalvoda E, Glasser BJ, Khinast JG. Mixing characteristics of wet granular matter in a bladed mixer. *Powder Technol*. 2010; 200:171–189.
33. Laurent BFC, Bridgwater J. Performance of single and six-bladed powder mixers. *Chem Eng Sci*. 2002;57:1695–1709.
34. Portillo PM, Muzzio FJ, Ierapetritou MG. Characterizing powder mixing processes utilizing compartment models. *Int J Pharmaceut*. 2006;320:14–22.
35. Pinson D, Zou RP, Yu AB, Zulli P, McCarthy MJ. Coordination number of binary mixtures of spheres. *J Physics D: Appl Phys*. 1998;31:457–462.
36. Porion P, Sommier N, Evesque P. Dynamics of mixing and segregation processes of grains in 3D blender by NMR imaging investigation. *Europhys Lett*. 2000;50:319–325.
37. Jain N, Ottino JM, Lueptow RM. Regimes of segregation and mixing in combined size and density granular systems: an experimental study. *Granular Matter*. 2005;7:69–81.

Manuscript received Aug. 17, 2010, revision received Feb. 25, 2011, and final revision received Apr. 7, 2011.